Ground-state and spectral signatures of cavity exciton-polariton condensates

Van-Nham Phan
Institute of Research and Development, Duy Tan University, K7/25 Quang Trung, Danang, Vietnam

Klaus W. Becker
Institut für Theoretische Physik, Technische Universität Dresden, D-01062 Dresden, Germany

Holger Fehske
Institut für Physik, Ernst-Moritz-Arndt-Universität Greifswald, D-17489 Greifswald, Germany
(Received 2 June 2015; revised manuscript received 13 January 2016; published 19 February 2016)

We propose a projector-based renormalization framework to study exciton-polariton Bose-Einstein condensation in a microcavity matter-light system. Treating Coulomb interaction and electron-hole/photon coupling effects on an equal footing, we analyze the ground-state properties of the exciton-polariton model according to the detuning and the excitation density. We demonstrate that the condensate by its nature shows a crossover from an excitonic insulator (of Bose-Einstein, respectively, BCS type) to a polariton and finally photonic condensed state as the excitation density increases at large detuning. If the detuning is weak, polariton or photonic phases dominate. While in both cases a notable renormalization of the quasiparticle band structure occurs that strongly affects the coherent part of the excitonic luminescence, the incoherent wave-vector-resolved luminescence spectrum develops a flat bottom only for small detuning.

DOI: 10.1103/PhysRevB.93.075138

I. INTRODUCTION

For several decades, there has been a considerable research effort to find Bose-Einstein condensation (BEC) in a solid-state system [1,2]. That excitons in semiconductors might condense into a macroscopic phase-coherent ground state was theoretically proposed about 50 years ago [3,4]. Experimentally, this has proved challenging, mainly because excitons are normally formed by optical excitations, and a cold degenerate Bose gas of sufficiently high density needs to be prepared on a shorter time scale than the excitons can decay in Ref. [5]. At high densities, however, very efficient exciton-exciton annihilation processes set in whose rates scale with the square of the exciton density. As a result, to date, all attempts to create a dense gas of excitons in a bulk crystal, e.g., in Cu_2O, or in a potential trap did not demonstrate conclusively excitonic BEC (for a recent review, see, e.g. Ref. [6]).

Different from optically created exciton condensates, the exciton insulator (EI) constitutes a quantum condensed state in equilibrium [7–9]. In this case, at low temperatures, electronic correlations can cause an anomaly at the semimetal-semiconductor transition that triggers an excitonic instability where the conventional ground state of the crystal becomes unstable with respect to the spontaneous formation of excitons. Depending on from which side of the semimetal-semiconductor transition the EI is approached, the EI typifies either as a BCS condensate of loosely bound electron-hole pairs or as a Bose-Einstein condensate of preformed tightly bound excitons [10,11]. Although there are some EI materials under debate [12–14], again we have no positive experimental proof of such an excitonic condensate.

In contrast, polaritons in semiconductor microcavities have been observed to exhibit BEC [15,16]. These experiments have been performed in the low-density regime; the polaritons are nonetheless not ideal (noninteracting) bosons. Besides, the polariton system is neither conservative nor in thermal equilibrium with the phonon (heat) bath. Even so, semiconductor exciton polaritons constitute a promising system to explore the physics of Bose gases, but in a stronger interaction regime [17]. Thereby, the excitonic (bound electron-hole pair) “matter” component and the strongly confined (photon-field) “light” component should be preferably treated on an equal footing. Likewise, the cases of low- and high-excitation densities should be described in a consistent scheme. Thereby the relationship between a polariton BEC, polariton, and photon lasing has to be clarified [18,19]. Here, a natural way is to analyze the luminescence spectrum of the system [20–22].

In this work, we investigate a many-body Hamiltonian describing a coupled electron-hole/photon system in a microcavity. In addition to the lattice periodic potential, the electrons and holes experience a Coulomb interaction and a coupling to the light field. In the past, mean-field theories have been used to study the limits of low-excitation densities [23] and high-excitation densities [24] separately. An extension to the medium-density regime has been addressed more recently by use of a variational (mean-field) treatment [18]. Here, we employ a projector-based renormalization method (PRM) [25–27] that allows to incorporate fluctuation processes beyond mean field in the entire excitation density range and treats the Coulomb interaction on an equal footing with the light-matter coupling. Moreover, depending on the bare band structure (semiconducting or semimetallic) and the detuning, we can address the formation of (BEC- or BCS-type) excitonic (insulator) phases, polariton and photonic condensates. Assuming that the polariton lifetime is longer than the thermalization time, we will first analyze the ground-state properties of the microcavity polariton system [18,28]. Since the PRM permits the calculation of spectral properties as well, in a second step, we will evaluate the excitonic luminescence. The paper is organized as follows. In Sec. II, we will introduce the exciton-polariton model and present its mean-field solution to set the stage for the more elaborate PRM treatment outlined in Sec. III. Details of the PRM calculation can be found in the Appendixes. The numerical results are discussed in Sec. IV.

Here, in particular, the behavior of the excitonic/photonic order parameters will be diagramed, just as the particle/photon excitation densities. Moreover, the luminescence spectra will be presented, both wave-vector resolved and integrated. Section V contains a brief summary and our main conclusions.

II. EXCITON-POLARITON MODEL

In the following, we study a model Hamiltonian for a polariton system in a semiconductor microcavity, which is in thermal equilibrium. Although experiments are usually performed away from equilibrium, there are reasons also to study the stationary state of a closed microcavity polariton system which appears to be well described by its ground state [18]. On the one hand, the quality of microcavity fabrication and of mirrors will improve, so that the experimental situation becomes closer to thermal equilibrium. On the other hand, thermal equilibrium may be considered as the limiting case of a nonequilibrium situation. This is the case when the decay rates for the loss of cavity photons and of fermions, for instance due to phonons or impurities, into external bath variables become small [28,29].

A model which is commonly used to describe such a microcavity polariton system is based on the Hamiltonian [18]

$$\mathcal{H} = \mathcal{H}_{\text{el}} + \mathcal{H}_{\text{ph}} + \mathcal{H}_{\text{el-ph}} + \mathcal{H}_{\text{el-el}}. \tag{1}$$

The first term $\mathcal{H}_{\text{el}}$ considers spinless free conduction electrons and valence holes with creation and annihilation operators $e^{(\dagger)}_{\mathbf{k}}, h^{(\dagger)}_{\mathbf{k}}$:

$$\mathcal{H}_{\text{el}} = \sum_{\mathbf{k}} \varepsilon^e_{\mathbf{k}} e^\dagger_{\mathbf{k}} e_{\mathbf{k}} + \sum_{\mathbf{k}} \varepsilon^h_{\mathbf{k}} h^\dagger_{\mathbf{k}} h_{\mathbf{k}}\,, \tag{2}$$

$$\varepsilon^e_{\mathbf{k}} = -2t \sum_i^D \cos k_i + \frac{E_g + 4tD - \mu}{2} = \varepsilon^h_{\mathbf{k}}\,, \tag{3}$$

where symmetric tight-binding dispersions $\varepsilon^e_{\mathbf{k}} = \varepsilon^h_{\mathbf{k}}$ for the respective excitation energies were assumed. In Eq. (3), t denotes the particle transfer amplitude, E_g gives the minimum distance (gap) between the bare electron and hole bands, and D is the dimension of the hypercubic lattice. Note that a semimetallic setting occurs when $E_g < 0$.

The second term $\mathcal{H}_{\text{ph}}$ is the free-photon Hamiltonian with photon creation (annihilation) operators $\psi^\dagger_{\mathbf{q}}$ ($\psi_{\mathbf{q}}$):

$$\mathcal{H}_{\text{ph}} = \sum_{\mathbf{q}} \omega_{\mathbf{q}} \psi^\dagger_{\mathbf{q}} \psi_{\mathbf{q}}, \tag{4}$$

$$\omega_{\mathbf{q}} = \sqrt{(c\mathbf{q})^2 + \omega_c^2} - \mu\,. \tag{5}$$

Here, $\omega_{\mathbf{q}}$ is the photonic excitation energy with a zero-point cavity frequency ω_c, and c is the speed of light in the microcavity.

The last two terms in Hamiltonian (1) are a local (attractive) Coulomb interaction between electrons and holes and a local interaction between the electron-hole system and photons with coupling constant g:

$$\mathcal{H}_{\text{el-el}} = -\frac{U}{N} \sum_{\mathbf{k}} \rho^e_{\mathbf{k}} \rho^h_{-\mathbf{k}}\,, \tag{6}$$

$$\mathcal{H}_{\text{el-ph}} = -\frac{g}{\sqrt{N}} \sum_{\mathbf{qk}} [e^\dagger_{\mathbf{k}+\mathbf{q}} h^\dagger_{-\mathbf{k}} \psi_{\mathbf{q}} + \text{H.c.}], \tag{7}$$

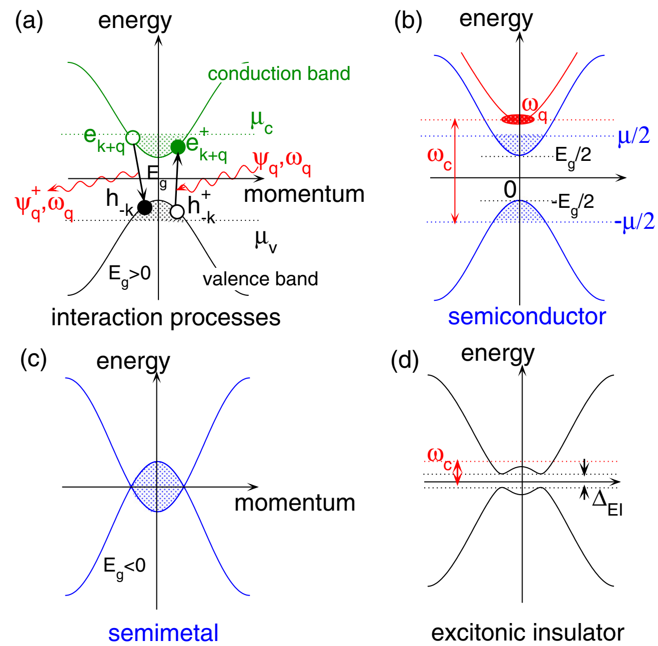

FIG. 1. Microcavity exciton-polariton model (1) studied in this work. Panel (a) represents the light-matter interaction processes taken into account. Panel (b) gives the band structure and relevant energy scales for a semiconducting situation. In panels (c) and (d), a semimetal with $E_g < 0$ (overlapping bands) is realized which might exhibit an excitonic instability that transforms the systems into an excitonic insulator [26].

where densities for electrons and holes have been introduced $\rho^e_{\mathbf{k}} = \sum_{\mathbf{k}_1} e^\dagger_{\mathbf{k}+\mathbf{k}_1} e_{\mathbf{k}_1}$ and $\rho^h_{\mathbf{k}} = \sum_{\mathbf{k}_1} h^\dagger_{\mathbf{k}+\mathbf{k}_1} h_{\mathbf{k}_1}$. In principle, additional electron-electron and hole-hole Coulomb interactions might have been taken into account in Eq. (6). However, they only lead to mere shifts in the one-particle dispersions $\varepsilon^e_{\mathbf{k}}$ and $\varepsilon^h_{\mathbf{k}}$ since spinless electrons and holes as well as a wave-vector-independent Coulomb coupling U are considered in model (1).

Note that in Eqs. (3) and (5) a chemical potential μ was included to ensure that the total number of excitations

$$\mathcal{N}_{\text{exc}} = \sum_{\mathbf{q}} \psi^\dagger_{\mathbf{q}} \psi_{\mathbf{q}} + \frac{1}{2} \sum_{\mathbf{k}} (e^\dagger_{\mathbf{k}} e_{\mathbf{k}} + h^\dagger_{\mathbf{k}} h_{\mathbf{k}}) \tag{8}$$

is fixed. Clearly, $\mathcal{N}_{\text{exc}}$ is conserved for Hamiltonian $\mathcal{H}$.

Apparently, the influence of $\mathcal{H}_{\text{el-ph}}$ becomes most important when the excitation energy of a particle-hole pair roughly agrees with a photon excitation. Therefore, for later interpretation of this effect one best introduces the so-called detuning parameter [18]

$$d = \omega_c - E_g\,. \tag{9}$$

Figure 1 illustrates the model under consideration.

Let us proceed by separating the mean-field approximation from model (1). Introducing the normal ordering for the operator expressions in $\mathcal{H}_{\text{el-el}}$ and $\mathcal{H}_{\text{el-ph}}$:

$$\begin{aligned} &: e^\dagger_{\mathbf{k}_1+\mathbf{k}} e_{\mathbf{k}_1} h^\dagger_{\mathbf{k}_2-\mathbf{k}} h_{\mathbf{k}_2} : \\ &= e^\dagger_{\mathbf{k}_1+\mathbf{k}} e_{\mathbf{k}_1} h^\dagger_{\mathbf{k}_2-\mathbf{k}} h_{\mathbf{k}_2} - \delta_{\mathbf{k},0} \big(n^e_{\mathbf{k}_1} : h^\dagger_{\mathbf{k}_2} h_{\mathbf{k}_2} : + n^h_{\mathbf{k}_2} : e^\dagger_{\mathbf{k}_1} e_{\mathbf{k}_1} : \big) \\ &- \delta_{\mathbf{k}_1,-\mathbf{k}_2} \big(d_{\mathbf{k}_1+\mathbf{k}} : h_{-\mathbf{k}_1} e_{\mathbf{k}_1} : + d_{\mathbf{k}_1} : e^\dagger_{\mathbf{k}_1+\mathbf{k}} h^\dagger_{-\mathbf{k}_1-\mathbf{k}} : \big), \end{aligned} \tag{10}$$

$$: e^\dagger_{\mathbf{q}+\mathbf{k}} h^\dagger_{-\mathbf{k}} \psi_{\mathbf{q}} : \\ = e^\dagger_{\mathbf{q}+\mathbf{k}} h^\dagger_{-\mathbf{k}} \psi_{\mathbf{q}} - \delta_{\mathbf{q},0}(d_{\mathbf{k}} : \psi_0 : + \langle \psi_0 \rangle : e^\dagger_{\mathbf{k}} h^\dagger_{-\mathbf{k}} :). \tag{11}$$

Hamiltonian (1) is rewritten as

$$\mathcal{H} = \mathcal{H}_0 + \mathcal{H}_1 \tag{12}$$

with

$$\mathcal{H}_0 = \sum_{\mathbf{k}} \hat{\varepsilon}^e_{\mathbf{k}} e^\dagger_{\mathbf{k}} e_{\mathbf{k}} + \sum_{\mathbf{k}} \hat{\varepsilon}^h_{\mathbf{k}} h^\dagger_{\mathbf{k}} h_{\mathbf{k}} + \sum_{\mathbf{q}} \omega_{\mathbf{q}} \psi^\dagger_{\mathbf{q}} \psi_{\mathbf{q}} \\ + \Delta \sum_{\mathbf{k}} (e^\dagger_{\mathbf{k}} h^\dagger_{-\mathbf{k}} + \text{H.c.}) + (\sqrt{N}\Gamma \psi^\dagger_0 + \text{H.c.}), \tag{13}$$

$$\mathcal{H}_1 = -\frac{g}{\sqrt{N}} \sum_{\mathbf{kq}} (: e^\dagger_{\mathbf{q}+\mathbf{k}} h^\dagger_{-\mathbf{k}} \psi_{\mathbf{q}} : + \text{H.c.}) \\ - \frac{U}{N} \sum_{\mathbf{k}_1\mathbf{k}_2\mathbf{k}} : e^\dagger_{\mathbf{k}_1+\mathbf{k}} e_{\mathbf{k}_1} h^\dagger_{\mathbf{k}_2-\mathbf{k}} h_{\mathbf{k}_2} : . \tag{14}$$

Additional constants have been neglected. In $\mathcal{H}_0$ the electronic excitation energies have acquired Hartree shifts

$$\hat{\varepsilon}^e_{\mathbf{k}} = \varepsilon^e_{\mathbf{k}} - \frac{U}{N} \sum_{\mathbf{q}} n^h_{\mathbf{q}}, \tag{15}$$

$$\hat{\varepsilon}^h_{\mathbf{k}} = \varepsilon^h_{\mathbf{k}} - \frac{U}{N} \sum_{\mathbf{q}} n^e_{\mathbf{q}}, \tag{16}$$

with

$$n^e_{\mathbf{k}} = \langle e^\dagger_{\mathbf{k}} e_{\mathbf{k}} \rangle, \quad n^h_{\mathbf{k}} = \langle h^\dagger_{\mathbf{k}} h_{\mathbf{k}} \rangle. \tag{17}$$

The last two contributions in $\mathcal{H}_0$ are additional fields with prefactors which will act below as order parameters for the exciton-polariton condensate:

$$\Delta = -\frac{g}{\sqrt{N}} \langle \psi_0 \rangle - \frac{U}{N} \sum_{\mathbf{k}} d_{\mathbf{k}}, \tag{18}$$

$$\Gamma = -\frac{g}{N} \sum_{\mathbf{k}} d_{\mathbf{k}}, \tag{19}$$

$$d_{\mathbf{k}} = \langle e^\dagger_{\mathbf{k}} h^\dagger_{-\mathbf{k}} \rangle = \langle h_{-\mathbf{k}} e_{\mathbf{k}} \rangle = d^*_{\mathbf{k}}. \tag{20}$$

Note that Hamiltonian $\mathcal{H} = \mathcal{H}_0 + \mathcal{H}_1$, with $\mathcal{H}_0$ and $\mathcal{H}_1$ given by Eqs. (13) and (14), is still exact. The mean-field approximation is obtained by completely neglecting the fluctuation part $\mathcal{H}_1$, i.e., $\mathcal{H}_{\text{MF}} = \mathcal{H}_0$. However, in the following we are mostly interested in the influence of fluctuation contributions to the physical behavior of an exciton-polariton condensate. Therefore, Hamiltonian $\mathcal{H}_1$ has to be taken into account.

Expression (13) for $\mathcal{H}_0$ can be further simplified since the terms $\propto \psi^\dagger_0$ and $\propto \psi_0$ can be eliminated by defining new displaced photon operators

$$\Psi^\dagger_{\mathbf{q}} = \psi^\dagger_{\mathbf{q}} + \frac{\sqrt{N}\Gamma}{\omega_{\mathbf{q}=\mathbf{0}}} \delta_{\mathbf{q},\mathbf{0}} . \tag{21}$$

Then,

$$\mathcal{H}_0 = \sum_{\mathbf{k}} \hat{\varepsilon}^e_{\mathbf{k}} e^\dagger_{\mathbf{k}} e_{\mathbf{k}} + \sum_{\mathbf{k}} \hat{\varepsilon}^h_{\mathbf{k}} h^\dagger_{\mathbf{k}} h_{\mathbf{k}} + \sum_{\mathbf{q}} \omega_{\mathbf{q}} \Psi^\dagger_{\mathbf{q}} \Psi_{\mathbf{q}} \\ + \Delta \sum_{\mathbf{k}} (e^\dagger_{\mathbf{k}} h^\dagger_{-\mathbf{k}} + \text{H.c.}) \tag{22}$$

and

$$\mathcal{H}_1 = -\frac{g}{\sqrt{N}} \sum_{\mathbf{kq}} [: e^\dagger_{\mathbf{q}+\mathbf{k}} h^\dagger_{-\mathbf{k}} \Psi_{\mathbf{q}} : + \text{H.c.}] \\ - \frac{U}{N} \sum_{\mathbf{k}_1\mathbf{k}_2\mathbf{k}} : e^\dagger_{\mathbf{k}_1+\mathbf{k}} e_{\mathbf{k}_1} h^\dagger_{\mathbf{k}_2-\mathbf{k}} h_{\mathbf{k}_2} : , \tag{23}$$

where the shift from Eq. (21) cancels in the first normal order product term of $\mathcal{H}_1$. Moreover, the electronic part of $\mathcal{H}_0$ can be diagonalized by means of a Bogoliubov transformation (compare Appendix A).

III. INFLUENCE OF FLUCTUATION PROCESSES

In mean-field treatment fluctuation processes from $\mathcal{H}_1$ are completely neglected. In the following, we apply the projective renormalization method [25] (PRM) in order to evaluate the order parameters, the electron and photon densities, and the response functions $A(\mathbf{k},\omega)$ and $B(\mathbf{q},\omega)$ of the exciton polarization and the cavity photon mode, respectively, for the case that $\mathcal{H}_1$ is included. The technical details of this calculation are shifted to Appendix B. The general concept of the PRM is as follows: the presence of the interaction $\mathcal{H}_1$ usually prevents a straightforward solution of the Hamiltonian $\mathcal{H} = \mathcal{H}_0 + \mathcal{H}_1$. However, by integrating out the interaction $\mathcal{H}_1$, the Hamiltonian can be transformed into a diagonal (or at least quasidiagonal) form by applying a sequence of small unitary transformations to $\mathcal{H}$. Denoting for a moment the corresponding generator of the whole sequence by $X = -X^\dagger$, it is shown in Appendix B how one arrives at an effective Hamiltonian $\tilde{\mathcal{H}} = e^X \mathcal{H} e^{-X}$, which has the same operator structure as Hamiltonian $\mathcal{H}_0$ from Eq. (22):

$$\tilde{\mathcal{H}} = \sum_{\mathbf{k}} \tilde{\varepsilon}^e_{\mathbf{k}} e^\dagger_{\mathbf{k}} e_{\mathbf{k}} + \sum_{\mathbf{k}} \tilde{\varepsilon}^h_{\mathbf{k}} h^\dagger_{\mathbf{k}} h_{\mathbf{k}} + \sum_{\mathbf{q}} \tilde{\omega}_{\mathbf{q}} \tilde{\Psi}^\dagger_{\mathbf{q}} \tilde{\Psi}_{\mathbf{q}} \\ + \sum_{\mathbf{k}} \tilde{\Delta}_{\mathbf{k}} (e^\dagger_{\mathbf{k}} h^\dagger_{-\mathbf{k}} + \text{H.c.}). \tag{24}$$

Here, $\tilde{\Psi}^\dagger_{\mathbf{q}}$ is defined by $\tilde{\Psi}^\dagger_{\mathbf{q}} = \psi^\dagger_{\mathbf{q}} + (\sqrt{N}\tilde{\Gamma}/\tilde{\omega}_{\mathbf{q}=\mathbf{0}})\delta_{\mathbf{q},\mathbf{0}}$ and $\tilde{\varepsilon}^e_{\mathbf{k}}, \tilde{\varepsilon}^h_{\mathbf{k}}, \tilde{\omega}_{\mathbf{q}}$, and $\tilde{\Delta}_{\mathbf{k}}$ are parameters which are renormalized in the elimination process. They have to be determined self-consistently by taking into account contributions to infinite order in the interaction $\mathcal{H}_1$. The PRM ensures a well-controlled disentanglement of higher-order interaction terms within the elimination procedure.

We would like to emphasize that the renormalized quantities $\tilde{\Delta}_{\mathbf{k}}$ just as $\tilde{\Gamma}$ in $\Psi_{\mathbf{q}}$ play the role of exciton-polariton order parameters for the full system (1). Thereby, both types of interactions contribute. In particular, both $\mathcal{H}_{\text{el-ph}}$ and $\mathcal{H}_{\text{el-el}}$ make contributions to $\tilde{\Delta}_{\mathbf{k}}$, where their mutual influence in the formation of a condensate will be of interest. On the other hand, the shift $\sim\tilde{\Gamma}$ in $\Psi_{\mathbf{q}}$ alone leads to a polarization of the photonic subsystem. In case the detuning parameter d [Eq. (9)] is small, the tendency for the formation of a photonic condensate is expected to be enhanced. In contrast, for large d the photonic contribution to $\tilde{\Delta}$ should be small, at least for a not too large excitation density $n_{\text{exc}} = \frac{1}{N}\langle \mathcal{N}_{\text{exc}} \rangle$.

The PRM also allows to evaluate expectation values $\langle \mathcal{A} \rangle$, formed with the full Hamiltonian $\mathcal{H}$. Thereby, one uses the property of unitary invariance of operator expressions under a trace. Employing the same unitary transformation to $\mathcal{A}$ as before to the Hamiltonian, one finds $\langle \mathcal{A} \rangle = \langle \tilde{\mathcal{A}} \rangle_{\tilde{\mathcal{H}}}$, where the expectation value on the right-hand side is now formed with $\tilde{\mathcal{H}}$, and $\tilde{\mathcal{A}} = e^X \mathcal{A} e^{-X}$. Just as $\mathcal{H}_0$ before also Hamiltonian $\tilde{\mathcal{H}}$ can be transformed into a diagonal form by a Bogoliubov transformation. Therefore, any expectation value, formed with $\tilde{\mathcal{H}}$, can be evaluated.

As a first example, let us consider the response function for the excitonic polarization $A(\mathbf{k},\omega)$, which is defined by the following linear response:

$$A(\mathbf{k},\omega) = \frac{1}{2\pi} \int_{-\infty}^{\infty} \langle [b_{\mathbf{k}}(t), b_{\mathbf{k}}^\dagger]_- \rangle \, e^{i\omega t} dt, \qquad (25)$$

with respect to an external $\mathbf{k}$- and ω-dependent field. Here, $b_{\mathbf{k}}^\dagger$ is the excitonic creation operator

$$b_{\mathbf{k}}^\dagger = \frac{1}{\sqrt{N}} \sum_{\mathbf{q}} e_{\mathbf{k}+\mathbf{q}}^\dagger h_{-\mathbf{q}}^\dagger. \qquad (26)$$

Applying the unitary invariance of operator expressions under a trace, $A(\mathbf{k},\omega)$ is rewritten as

$$A(\mathbf{k},\omega) = \frac{1}{2\pi} \int_{-\infty}^{\infty} \langle [\tilde{b}_{\mathbf{k}}(t), \tilde{b}_{\mathbf{k}}^\dagger]_- \rangle_{\tilde{\mathcal{H}}} \, e^{i\omega t} dt, \qquad (27)$$

where the expectation value is now formed with $\tilde{\mathcal{H}}$ instead of with $\mathcal{H}$. Correspondingly, $\tilde{b}_{\mathbf{k}}^{(\dagger)}$ are the transformed electron operators, $\tilde{b}_{\mathbf{k}}^{(\dagger)} = e^X b_{\mathbf{k}}^{(\dagger)} e^{-X}$, and the time dependence in Eq. (27) is governed by $\tilde{\mathcal{H}}$ as well. Explicit expressions for both coherent and incoherent contributions to $A(\mathbf{k},\omega)$ are derived in Appendix B.

We note that $A(\mathbf{k},\omega)$ is not a positive-definite spectral function. However, $A(\mathbf{k},\omega)$ divided by ω has a positive sign for all ω, i.e., $A(\mathbf{k},\omega)/\omega \geqslant 0$. The quantity $A(\mathbf{k},\omega)$ has the advantage that it fulfills a simple sum rule

$$\int_{-\infty}^{\infty} A(\mathbf{k},\omega) d\omega = \frac{1}{N} \sum_{\mathbf{k}'} \left[1 - \left(n_{\mathbf{k}'}^e + n_{\mathbf{k}'}^h\right)\right] \qquad (28)$$

(independent of $\mathbf{k}$), which will be used in the following to check the outcome of the numerics.

As a second example, we will evaluate the response function of the cavity photon mode, which is sometimes called just luminescence function

$$B(\mathbf{q},\omega) = \frac{1}{2\pi} \int_{-\infty}^{\infty} \langle [\psi_{\mathbf{q}}(t), \psi_{\mathbf{q}}^\dagger]_- \rangle \, e^{i\omega t} dt. \qquad (29)$$

Applying the unitary transformation it can be written as

$$B(\mathbf{q},\omega) = \frac{1}{2\pi} \int_{-\infty}^{\infty} \langle [\tilde{\psi}_{\mathbf{q}}(t), \tilde{\psi}_{\mathbf{q}}^\dagger]_- \rangle_{\tilde{\mathcal{H}}} \, e^{i\omega t} dt, \qquad (30)$$

where $\tilde{\psi}_{\mathbf{q}}^\dagger$ is the fully transformed photon mode. $B(\mathbf{q},\omega)$ will be evaluated in Appendix B as well. Note that $B(\mathbf{q},\omega)$ obeys the sum rule $\int_{-\infty}^{\infty} B(\mathbf{q},\omega) d\omega = 1$.

IV. NUMERICAL RESULTS

In the numerical evaluation of the various physical quantities from Sec. III one has to solve the set of renormalization equations (B12)–(B17) self-consistently together with the expressions (B50)–(B52) and (B59) for the expectation values.

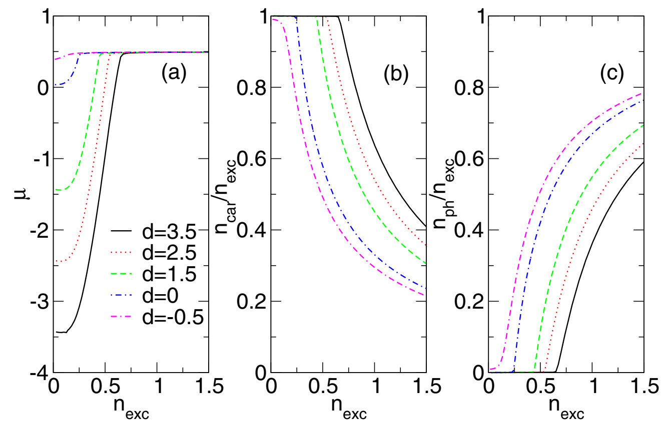

FIG. 2. Chemical potential μ (a), density of excitons n_X (b), and density of photons n_{ph} (c), as a function of the total excitation density for various detunings d. Model parameters are $U = 2$, $g = 0.2$, and $\omega_c = 0.5$.

Starting with some chosen initial values for $n_{\mathbf{k}}^e, n_{\mathbf{k}}^h, n_{\mathbf{q}}^\psi$, and $\Delta_{\mathbf{k}} = \Gamma = 0^+$, the renormalization equations are integrated in small steps $\Delta\lambda$ until at $\lambda = 0$ the Hamiltonian is completely renormalized. Then, the expectation values can be recalculated and the renormalization process is restarted again. Convergence is achieved if all quantities are determined within some relative error of, for instance, less than 10^{-5}. To simplify the numerics, we consider a one-dimensional setting hereafter, and limit the number of lattice sites to $N = 160$. Nevertheless, the results presented in the framework of the PRM approximation should also give a qualitative account of what happens in a higher-dimensional microcavity polariton system.

A. Ground-state properties

Assuming a quasiequilibrium situation, the ground state of the system can be determined for a fixed excitation density n_{exc} at zero temperature in dependence on the model parameters, i.e., according to the detuning d, the electron-hole Coulomb attraction U, and the light-matter coupling strength g. Here and in what follows, all energies are given in units of the particle transfer amplitude t and the wave vectors in units of the lattice constant a. For the explicit evaluation one best introduces a dimensionless speed of light $\bar{c}$ using $\hbar\omega_{\mathbf{q}}/t = [\bar{c}^2(\mathbf{q}/\pi)^2 + (\hbar\omega_c/t)^2]^{(1/2)} - (\hbar\mu/t)$ where $\bar{c} = (\hbar\pi/at)c$. Taking $\bar{c} = 80$ and typical values for $a \simeq 5$ Å and $t \simeq 2$ eV one is led to a value of $c \simeq 0.4\, c_0$ for the speed of light of the microcavity, which is about half the speed of light c_0 in vacuum. However, as we have noticed, most of the physical properties only slightly depend on the actual value of c.

Figure 2 shows how the chemical potential, the partial densities of carriers and photons vary as the total number (density) of excitations changes at $\omega_c = 0.5$, for detunings ranging from $d = 3.5$ ($E_g = -3$) to $d = -0.5$ ($E_g = 1$). Recall negative (positive) values of E_g lead to a semimetallic (semiconducting) bare band structure. As a matter of course, the chemical potential increases as the number of excitations increases [see Fig. 2(a)]. The weak variation at small n_{exc} is an effect of the van Hove singularity of the one-dimensional (1D) density of states, while the almost constant μ at large n_{exc}

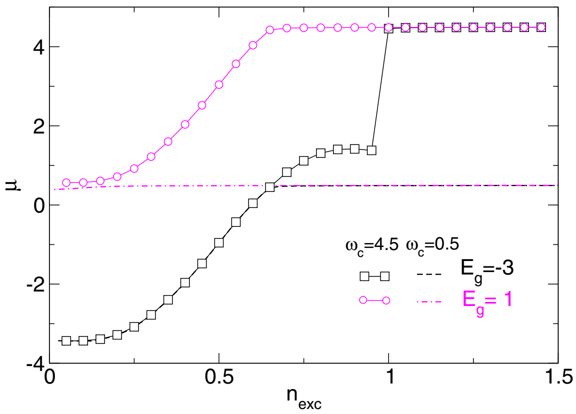

FIG. 3. Chemical potential μ as a function of the excitation density $n_{\rm exc}$ at fixed values of $E_g = 1$ and -3. Dashed lines mark the results for $\omega_c = 0.5$ [cf. Fig. 2(a)]; solid lines with symbols give the new data for $\omega_c = 4.5$, where $d = 3.5$ and 7.5 result for $E_g = 1$ and -3, respectively. The interaction parameters are $U = 2$ and $g = 0.2$.

can be traced back to conduction electron phase-space filling: If μ reaches ω_c, any further excitation (that minimizes the ground-state energy) will be photonic. The partial excitation densities of carriers and photons shown in Figs. 2(b) and 2(c), respectively, corroborate this scenario. We see that for large detuning the excitations in the low-density regime are basically electron-hole excitations. Thereby, the electrons and holes form an electron-hole plasma at weak-to-moderate values of U, or might bound into excitons in the strong-coupling regime. Increasing $n_{\rm exc}$, above a certain threshold value a sharp onset of photon excitations takes place, signaling laserlike behavior [18]. The electron-hole plasma, respectively, excitonic domain appearing at low density shrinks as the detuning becomes smaller and finally a very gradual (but still opposing) variation of $n_{\rm car}$ and $n_{\rm ph}$ is observed as $n_{\rm exc}$ increases. Obviously, now the quasiparticle excitations are a mixture of excitons and photons, i.e., they can be viewed as polaritons.

This scenario is corroborated by Fig. 3, which compares the variation of μ with $n_{\rm exc}$ for small ($\omega_c = 0.5$) and large ($\omega_c = 4.5$) values of the cavity frequency when the gap parameter E_g is kept fixed. For $E_g = -3$, yielding a large detuning in both low-ω_c and high-ω_c cases, the (continuous) $\mu(n_{\rm exc})$ dependence is almost the same until μ intersects the photon energy. As becomes clear from Fig. 2(a) for $\omega_c = 0.5$ no photon excitations are involved in the small $n_{\rm exc}$ regime below this intersection, which is also true for $\omega_c = 4.5$. Due to the same E_g and thus the same dispersion $\varepsilon^e_{\mathbf{k}} = \varepsilon^h_{\mathbf{k}}$ for both cases the curves μ as a function $n_{\rm exc}$ should be the same as long as μ is smaller than $\omega_c = 0.5$. If the cavity frequency is (much) larger than the width of the bare band structure, we observe a jump at $n_{\rm exc} = 1$. Here, all available electrons and holes are bound into excitons, i.e., any further excitation is purely photonic by their nature.

In order to analyze how Coulomb and light-matter interactions operate together establishing a quantum condensed state, we have separately determined the two (excitonic and photonic) contributions to the order parameter Δ on the right-hand side of Eq. (18): $\Delta_X = -\frac{U}{N}\sum_{\mathbf{k}} d_{\mathbf{k}}$ and $\Delta_{\rm ph} = -\frac{g}{\sqrt{N}}\langle\psi_0\rangle$.

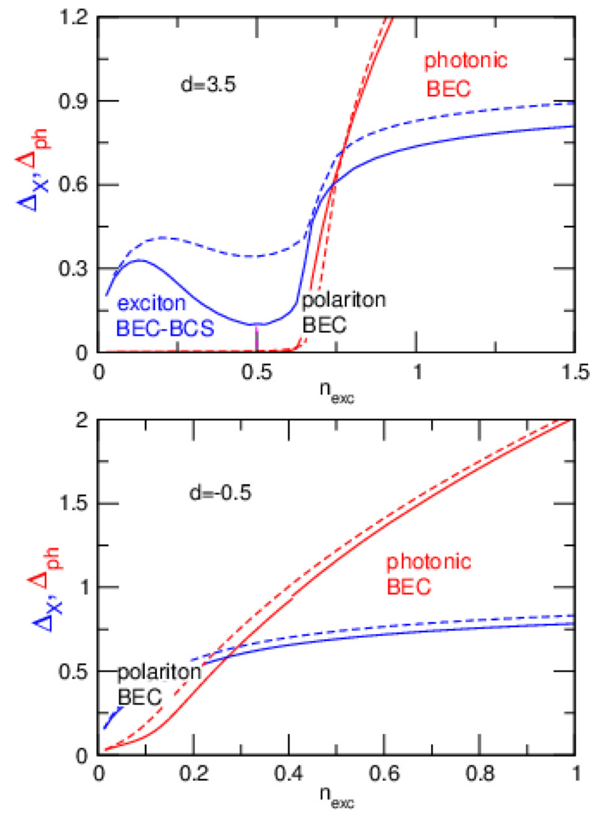

FIG. 4. Excitonic (Δ_X) and photonic ($\Delta_{\rm ph}$) order parameters as a function of the excitation density $n_{\rm exc}$ at large (upper panel) and small (lower panel) detuning d. Different phases refer to the predominant nature of the condensate. Parameters are $U = 2$, $g = 0.2$, and $\omega_c = 0.5$. The dashed lines give the corresponding results in the mean-field approximation (see Appendix A), which naturally overestimates the tendency towards the formation of condensed phases.

The results are shown in Fig. 4. For large detuning (upper panel), an excitonic condensate is formed at low densities (note that the photonic order parameter vanishes). For the U value $U = 2$ considered here it typifies a BEC of preformed electron-hole pairs. As the excitation density increases, phase-space (Pauli-blocking) effects become more and more important (see following) and the condensate becomes BCS type, but still the light component is negligible. Increasing the density further photonic effects came into play. As a result, the condensate turns from excitonic to polaritonic. At even higher excitation densities, the excitonic component saturates, whereas the photonic order parameter continues its increase. This classifies a photonic condensate. For smaller detuning but fixed ω_c, both excitonic and photonic order parameters are intimately connected in the whole low-to-intermediate excitation density regime, indicating a polariton BEC, which again gives way to photonic BEC at very large $n_{\rm exc}$. Of course, by their nature, all these transitions are crossovers.

Figures 5 and 6 give the wave-vector-resolved intensity of the electron-hole pair order-parameter function $d_{\mathbf{k}}$ [Eq. (B49)] and the photon density $\langle\psi^\dagger_{\mathbf{q}}\psi_{\mathbf{q}}\rangle$ [Eq. (B54)], respectively. For large detuning $d = 3.5$, Fig. 5 indicates how the maximum of the pairing amplitude $d_{\mathbf{k}}$ is continuously shifted from $k = 0$ at $n_{\rm exc} \ll 1$ to larger values of k as $n_{\rm exc}$ is raised,

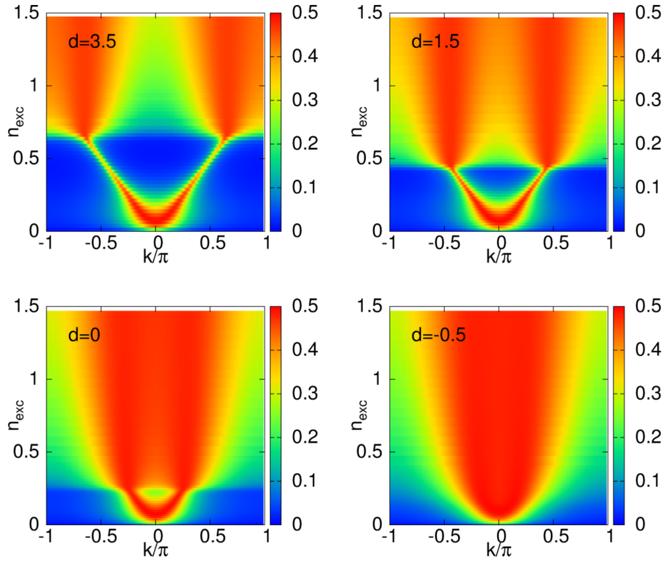

FIG. 5. Intensity plot of the electron-hole-pairing amplitude $d_{\mathbf{k}}$ in the momentum-density plane at different detuning d, for $U = 2$, $g = 0.2$, and $\omega_c = 0.5$.

which reveals finite density (Pauli-blocking) effects. Above a "critical" density $n_{\rm exc} \simeq 0.66$ (cf. also Fig. 3), where $\mu \simeq \omega_c$, the photon field comes into play (cf. Fig. 6 left upper panel). Simultaneously, the renormalization of the band structure due to the Coulomb interaction (see following) leads to a high intensity of $d_{\mathbf{k}}$ at large momenta ($|\mathbf{k}| > \pi/2$). For small detuning $d = -0.5$, the light-matter coupling affects the behavior of $d_{\mathbf{k}}$ from the very beginning ($n_{\rm exc} \to 0$), yielding a strong polariton signature around $k = 0$ which broadens at higher excitation densities. Clearly, the intensity of the photon field is always peaked around $q = 0$ and comes up at larger excitation density the larger the detuning is (see Fig. 6).

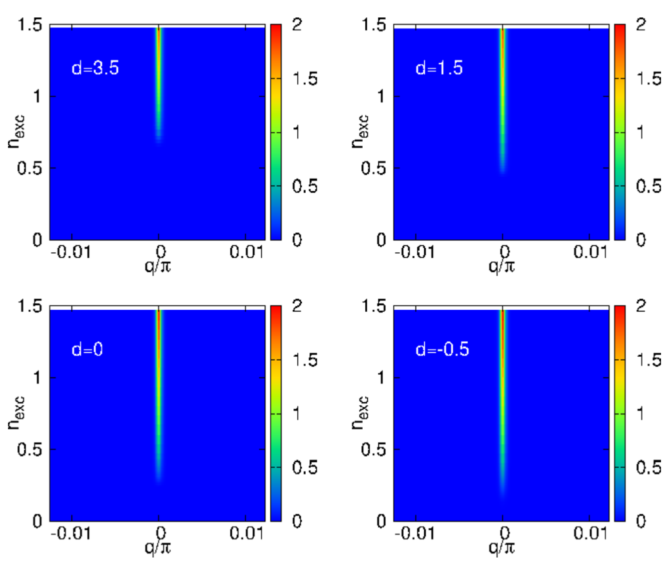

FIG. 6. Intensity plot of the photon density $\langle \psi_{\mathbf{q}}^{\dagger} \psi_{\mathbf{q}} \rangle$ in the momentum-density plane at different detuning d, for $U = 2$, $g = 0.2$, $\omega_c = 0.5$, and $T = 0.01$.

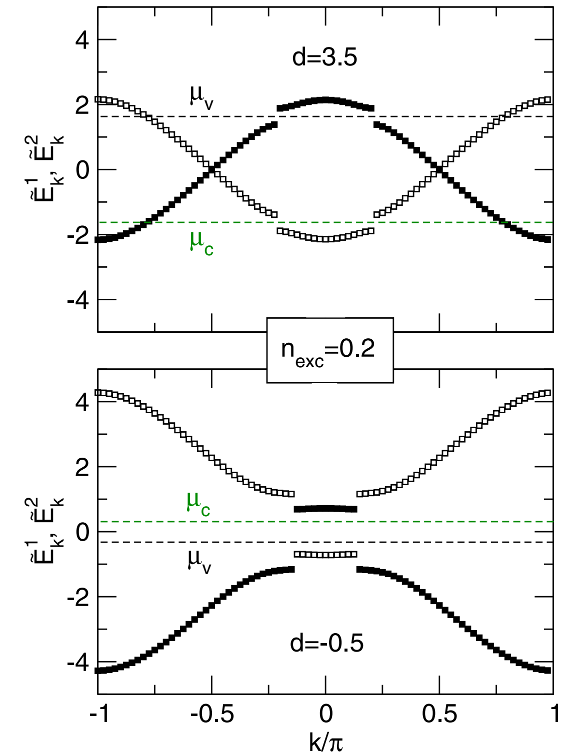

FIG. 7. Quasiparticle energies (B30) for large (upper panel) and small (lower panel) detuning at $n_{\rm exc} = 0.2$, where, $U = 2$, $g = 0.2$, and $\omega_c = 0.5$. Filled (open) symbols mark the valence (conduction) band with chemical potentials $\mu_v = -\mu/2$ ($\mu_c = \mu/2$).

Starting from the bare band structure (3), it will be interesting to look how the quasiparticle bands (B30) evolve, which are renormalized on account of Coulomb and light-matter interaction effects. Figure 7 gives $\tilde{E}_{\mathbf{k}}^{1,2}$ for $n_{\rm exc} = 0.2$. For large detuning ($d = 3.5$, $E_g = -3$), the bare bands interpenetrate [cf. Fig. 1(c)]. Here, basically all excitations are excitons (formed by the electrons and holes in the central part of the Brillouin zone). For small detuning ($d = -0.5$, $E_g = 1$), the (bare) semiconductor band structure [cf. Fig. 1(b)] is preserved. Again, excitonic bound states occur but not as many as for $d = 3.5$; instead, more photonic states contribute to $n_{\rm exc}$.

Figure 8 shows the renormalized "band structure" for different excitation densities; here valence and conduction bands were shifted by $-\mu_v$, respectively, $-\mu_c$. Of course, at $n_{\rm exc} = 0.001$ the dispersions are barely changed from those of the bare bands. However, in order to realize such a very small excitation densities at $d = 3.5$, $E_g = -3$, i.e., for strongly overlapping bare bands, a large negative value of μ arises [cf. Fig. 2(a)]. Increasing $n_{\rm exc}$, the location of the gap is shifted from $k = 0$ (as was the case for $n_{\rm exc} = 0.001$) to a finite k value. We find a band structure as for a BCS-type exciton insulator state [26] [cf. Fig. 1(d)]. For $n_{\rm exc} = 0.5$, a complete backfolding of the bands (doubling of the Brillouin zone) takes place. For this effect, the attractive Coulomb interaction between electrons and holes is responsible. The situation significantly changes at small detuning. Here, always a semiconductor band structure is observed, although the particle-photon coupling leads to a flattening of the top of

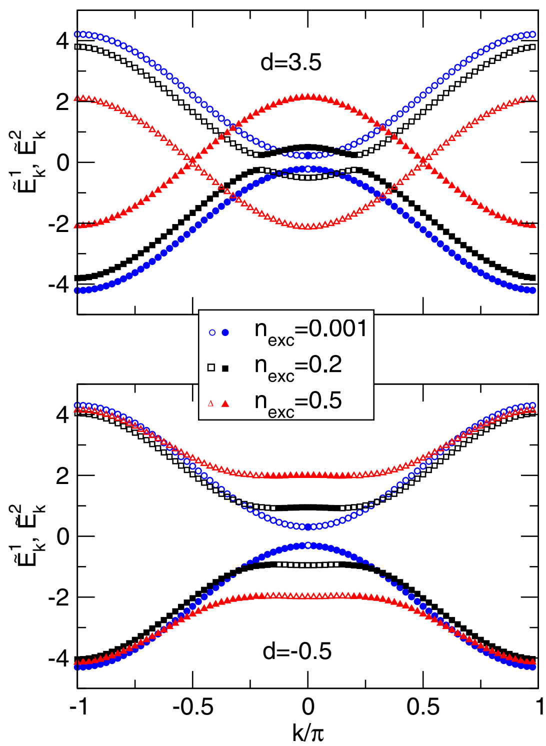

FIG. 8. Renormalized band structure (B30) for large (upper panel) and small (lower panel) detuning at various $n_{\rm exc}$. Note that now the energies of the valence bands (filled symbols) and conduction bands (open symbols) are measured from μ_v and μ_c, respectively. Again, $U = 2$, $g = 0.2$, and $\omega_c = 0.5$.

the valence band, respectively, bottom of the conduction band. As a result, the bandwidth of both bands shrinks and the gap broadens. This clearly can be attributed to the hybridization between electronic and photonic degrees of freedom in the course of polariton formation.

Let us now discuss the ground-state properties in dependence on the Coulomb and light-matter interaction strengths. Figure 9 gives the variation of Δ_X and $\Delta_{\rm ph}$ with U. For large detuning and small excitation density, electron-hole pairing starts above a certain Coulomb interaction threshold with states involved that are close to the Fermi momenta. We find almost no photonic contribution in this case. Hence, the coherent state classifies as an excitonic condensate. At larger excitation density polaritons are formed for small values of U (note that for $U = 0$ the condensate is completely triggered by the photons). Increasing U, the ground state becomes dominated by Coulomb correlations again, and we obtain an ordered state of tightly bound excitons (reminiscent of the excitonic insulator phase). At small detuning, the polariton BEC features finite excitonic and photonic order parameters, where the former (latter) is enhanced (suppressed) as U rises at fixed g, indicating a crossover from an excitonic to a photonic dominated ground-state wave function. The g dependence of the order parameters displayed in Fig. 10 demonstrates that both pairings Δ_X and $\Delta_{\rm ph}$ are always strengthened by increasing the light-matter coupling for both large and small detunings. In contrast, for decreasing $g \to 0$ only $\Delta_{\rm ph}$ vanishes, whereas Δ_X stays finite for large detuning

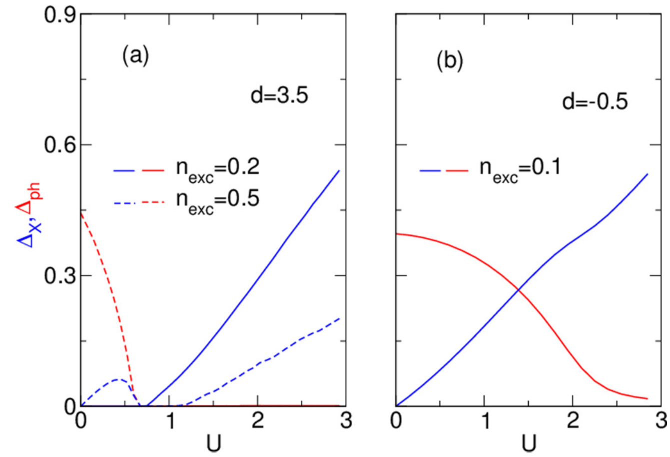

FIG. 9. Excitonic (blue lines) and photonic (red lines) order parameters as a function of U for the case of large detuning, $d = 3.5$ (left), and small detuning $d = -0.5$ (right), where $g = 0.2$ and $\omega_c = 0.5$.

but approaches zero for small detuning because we are in the polariton regime and $U = 2 \lesssim U_c$. Moreover, a slow saturation of Δ_X at large values of g is observed.

B. Spectral properties

The luminescence of the microcavity exciton-polariton system is first characterized by the intensity plots of $A(k,\omega)$; see Figs. 11 and 12 at $\omega_c = 0.5$, for the cases of large and small detuning, respectively. Here, ω and $\mathbf{k}$ denote the energy and momentum transfer. The left panels display the (dominant) coherent contributions (C4), resulting from electron-hole pair annihilation and creation processes inside and in-between the fully renormalized quasiparticle bands $\tilde{E}^{1,2}_{\mathbf{k}}$ [cf. Eq. (B30) and Figs. 7 and 8] without any additional photons involved. The less intense incoherent parts (C5) include higher-order exciton and photon contributions. Special attention deserves

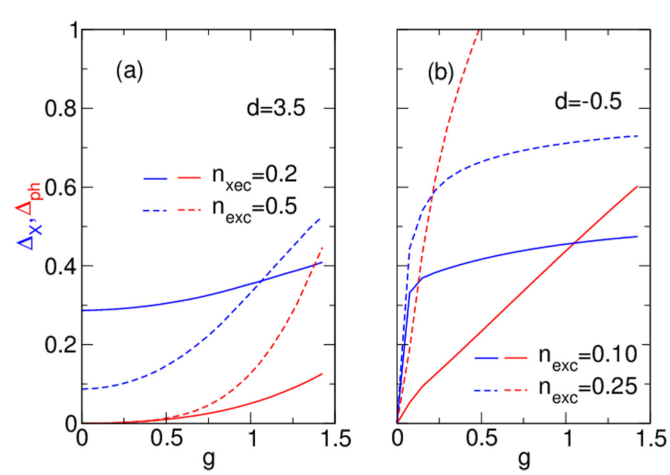

FIG. 10. Excitonic (blue lines) and photonic (red lines) order parameters as functions of g for the cases of large detuning $d = 3.5$ (left) and small detuning $d = -0.5$ (right), where $U = 2$ and $\omega_c = 0.5$ (note that $U = 2$ roughly equates the critical value for exciton formation at $g = 0$).

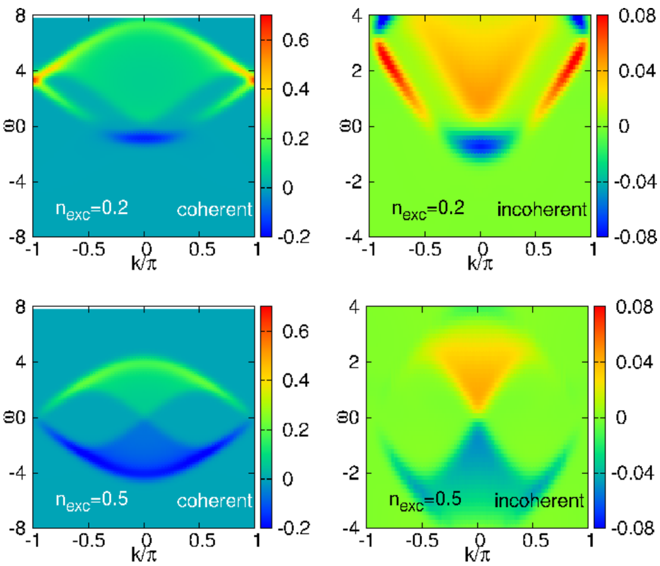

FIG. 11. Intensity plot of the excitonic polarization $A(\mathbf{k},\omega)$ for $n_{\rm exc} = 0.2$ (upper panels) and $n_{\rm exc} = 0.5$ (lower panels) at large detuning $d = 3.5$. Again, $U = 2$, $g = 0.2$, and $\omega_c = 0.5$. Here, the left panels refer to the coherent part $A^{\rm coh}(\mathbf{k},\omega)$, the right panels give the incoherent contribution $A^{\rm inc}(\mathbf{k},\omega)$.

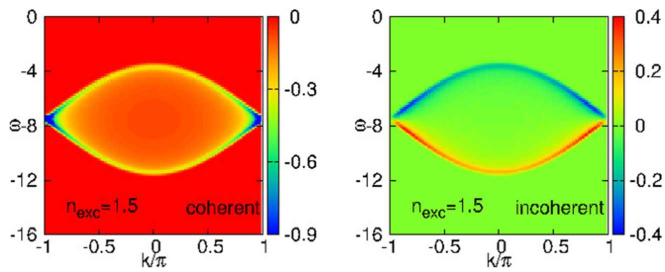

FIG. 13. Intensity plot of the excitonic polarization $A(\mathbf{k},\omega)$ for $n_{\rm exc} = 1.5$, where $U = 2$ and $g = 0.2$. Now, $\omega_c = 4.5$ and $E_g = -3$, resulting in a detuning $d = 7.5$.

the significant flattening of the excitonic response at small momentum transfer for small detuning, which is caused by a strong light-matter interaction and indicates the formation of an exciton-polariton condensate [6].

If the cavity frequency and the detuning are very large, a coherent signal for the excitonic polarization is obtained for negative ω only. Figure 13 displays $A(\mathbf{k},\omega)$ for $\omega_c = 4.5$ and $d = 7.5$ at large excitation density $n_{\rm exc} = 1.5$. We see that all available electrons and holes are paired into excitons, and the photonic excitations [not directly probed by $A(\mathbf{k},\omega)$] are energetically separated (cf. Fig. 3).

The total intensity of the excitonic polarization is given by

$$I(\omega) = \frac{1}{N}\sum_{\mathbf{k}} |S(\mathbf{k})|^2 A(\mathbf{k},\omega), \tag{31}$$

where the prefactor $|S(\mathbf{k})|^2$ is proportional to the exciton-photon interaction strength. For convenience will be set $|S(\mathbf{k})|^2 = g^2$. The quantity $I(\omega)$ is shown in Figs. 14 and 15 for $\omega_c = 0.5$ and 4.5, respectively for different excitation densities. Starting in Fig. 14 with small $n_{\rm exc}$, we observe a

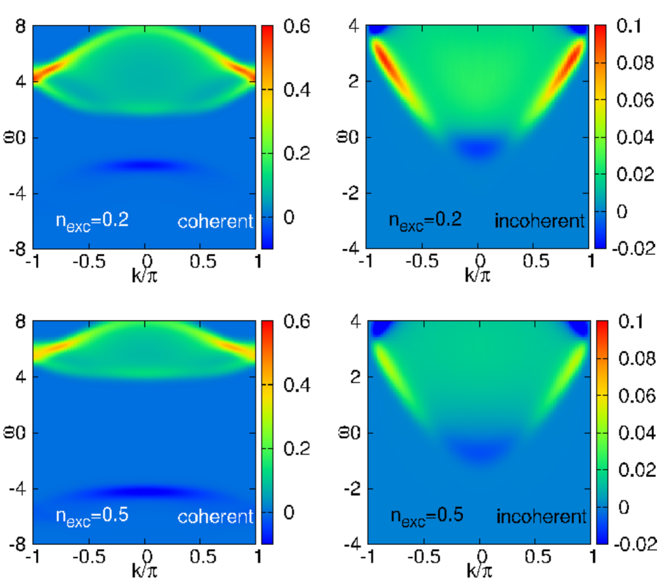

FIG. 12. Intensity plot of the excitonic polarization $A(\mathbf{k},\omega)$ for $n_{\rm exc} = 0.2$ (upper panels) and $n_{\rm exc} = 0.5$ (lower panels) at small detuning $d = -0.5$. Other parameters and notations as in Fig. 11.

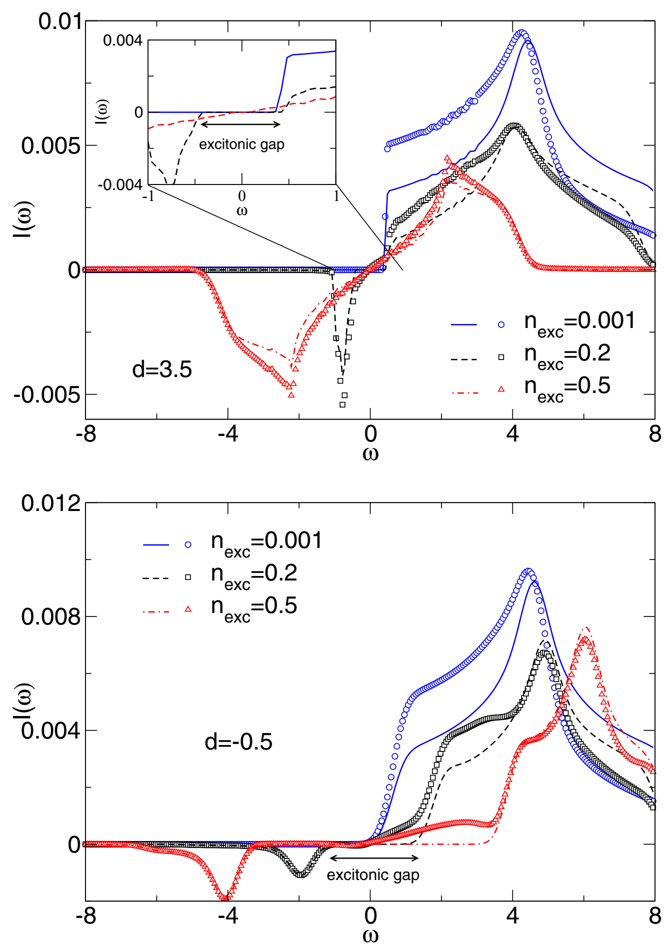

FIG. 14. Total excitonic intensity $I(\omega)$ for large detuning ($d = 3.5$, upper panel) and small detuning ($d = -0.5$, lower panel) at various $n_{\rm exc}$, where $U = 2$, $g = 0.2$, and $\omega_c = 0.5$.

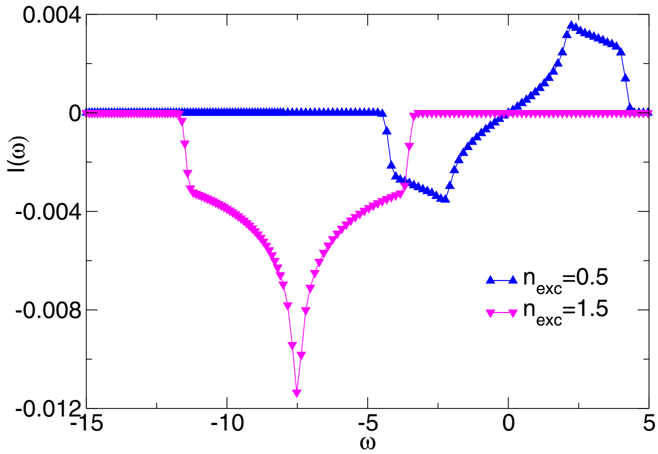

FIG. 15. Total excitonic intensity $I(\omega)$ for $n_{\mathrm{exc}} = 0.5$ and 1.5 at $\omega_c = 4.5$. Model parameters are $U = 2$, $g = 0.2$, and $E_g = -3$ ($d = 7.5$).

distinctly asymmetric line shape (with respect to $\omega \to -\omega$). The gap around $\omega = 0$ is an evidence for the formation of an exciton-polariton condensate, particularly for small detuning (see Fig. 14). For $\omega_c = 4.5$ (Fig. 15), excitonic and photonic excitations are well separated and the excitonic polarization intensity acquires a symmetric line shape. Note that $I(\omega)$ fulfills the sum rule (28).

Finally, we also consider the luminescence spectral function $B(\mathbf{q},\omega)$. The results for small and large detunings are shown in Figs. 16 and 17. In both cases, the coherent parts of the spectrum are dominant and follow the renormalized photon excitation $\omega_{\mathbf{q}}$, whereas the incoherent excitations are of minor importance. Note that because of the steep increase with $\mathbf{q}$ of the photonic dispersion $\omega_{\mathbf{q}}$ [Eq. (5)], Figs. 16 and 17 focus on the small-$\mathbf{q}$ interval around $\mathbf{q} = 0$. As anticipated from Appendix B, the onsets of the incoherent excitations of

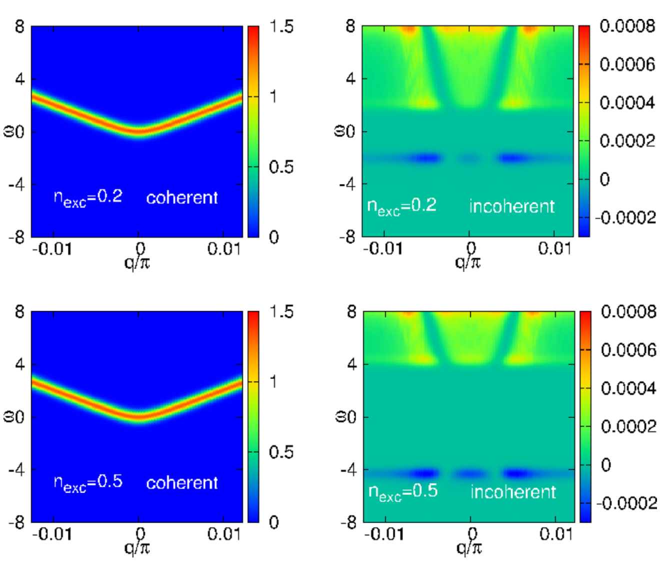

FIG. 16. Intensity plot of the luminescence spectral function $B(\mathbf{q},\omega)$ for $n_{\mathrm{exc}} = 0.2$ (upper panels) and $n_{\mathrm{exc}} = 0.5$ (lower panels) at small detuning $d = -0.5$. Other parameters and notations as in Fig. 12.

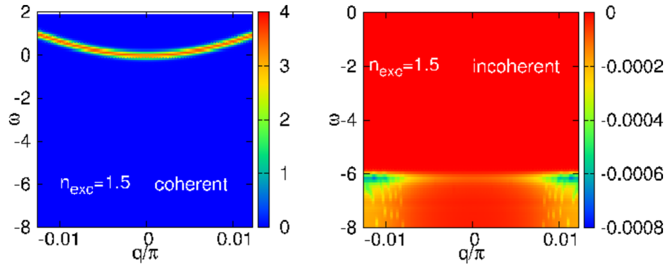

FIG. 17. Intensity plot of the luminescence function $B(\mathbf{q},\omega)$ for the same parameters as in Fig. 13.

$B(\mathbf{q},\omega)$ correspond to those of the coherent parts of $A(\mathbf{k},\omega)$. However, due to the restricted $\mathbf{q}$ range in Figs. 16 and 17, this equivalence is hardly seen except in the dark blue horizontal regions of low intensities in the right panels of Fig. 16 and the left panels of Fig. 10. Moreover, the spectral weights of the coherent excitations of $B(\mathbf{q},\omega)$ in Figs. 16 and 17 are almost independent of $\mathbf{q}$. However, there seems to be a contradiction to the outcome in Fig. 6. There, for a small $\omega_c = 0.5$, an intensity plot of the photon density $\langle \psi_{\mathbf{q}}^\dagger \psi_{\mathbf{q}} \rangle$ in momentum space is shown, revealing a strongly peaked intensity around $\mathbf{q} = 0$ only. This apparent contradiction can easily be resolved by help of the dissipation-fluctuation theorem:

$$\langle \psi_{\mathbf{q}}^\dagger \psi_{\mathbf{q}} \rangle = \int_{-\infty}^{\infty} d\omega \, \frac{B(\mathbf{q},\omega)}{e^{\beta\omega} - 1} \,. \tag{32}$$

Exploiting the fact that the coherent part of $B(\mathbf{q},\omega)$ is dominant $B(\mathbf{q},\omega) \approx |\tilde{z}_{\mathbf{q}}|^2 \, \delta(\omega - \tilde{\omega}_{\mathbf{q}})$ ($|\tilde{z}_{\mathbf{q}}|^2 \approx 1$), one finds

$$\langle \psi_{\mathbf{q}}^\dagger \psi_{\mathbf{q}} \rangle \approx |\tilde{z}_{\mathbf{q}}|^2 \, \frac{1}{e^{\beta\tilde{\omega}_{\mathbf{q}}} - 1} \,. \tag{33}$$

Obviously, for small temperatures (large β) wave vectors around $\mathbf{q} = 0$ contribute most since $\tilde{\omega}_{\mathbf{q}}$ is smallest there: This is particularly true for the case of Fig. 6, where a small zero-point cavity frequency $\omega_c = 0.5$ was used. When we calculate the expectation value $\langle \psi_{\mathbf{q}}^\dagger \psi_{\mathbf{q}} \rangle$ for a large photon frequency $\omega_c = 4.5$ (and $d = 7.5$), the intensity of the photon density is smeared out, of course, in momentum space (not shown).

V. CONCLUSIONS

To summarize, we have adapted the PRM (projective renormalization method) to investigate an exciton-polariton microcavity model with regard to the formation of Bose-Einstein condensates. Thereby, correlation and fluctuation effects were included. The PRM allows to derive analytical expressions for the excitonic and photonic (BEC) order parameters, the partial excitation densities of excitons and photons, the fully renormalized quasiparticle band structure, and the luminescence spectrum in the whole parameter regime of detuning, excitation density, Coulomb interaction, and light-matter coupling. The nature of the condensate changes from an exciton to a polariton and finally to a photon dominated ground state when the density of excitations grows. For large detuning, the exciton condensate shows a crossover from a BEC- to a BCS-type pairing, mainly because of Fermi-surface and Pauli-blocking effects. In this regime, also a clear onset density is observed for the photonic fraction, when the total excitation is increased. At the same time, the carrier density saturates. For small detuning, a strong mixture of electron and photon degrees of freedom takes place, right from starting to increase the excitation density. In this regime, pronounced polariton signatures can be found. The photonic (laserlike) behavior shows a smooth onset and dominates the physics at very large excitation densities. In this way, our more elaborated PRM approach confirms the exciton-polariton-photon crossover scenario obtained in the framework of a variational (mean-field) treatment [18]. The luminescence and excitonic polarization spectra presented for the different parameter regimes support this behavior of the microcavity system as well. To analyze the influence of a trap potential [6] on the excitonic luminescence would be a worthwhile goal of forthcoming studies. Equally interesting would be to extend the PRM scheme to the study of exciton-polariton systems in nonequilibrium, e.g., with a focus on the description of lasing.

Note that this study for the luminescence spectrum differs from those in literature on microcavity polaritons since there the exciton degrees of freedom are often described by local two-level systems (see for instance Refs. [29,30]). Instead, in this study a coherent set of conduction electrons and valence holes for the exciton degrees of freedom is considered which has strong influence on the excitonic polarization $A(\mathbf{k},\omega)$, though rather little influence on the luminescence function $B(\mathbf{q},\omega)$. On the other hand, in this study, the contributions of Goldstone modes to the spectra were neglected. In principle, they should show up since the continuous gauge symmetry $U(\alpha)\mathcal{H}U^{-1}(\alpha)=\mathcal{H}$ with $U(\alpha)=\exp(-i\alpha\mathcal{N}_{\rm exc})$ is violated in the condensed phase. Then, in a linearized equation of motion method, a coupled set of equations for the photonic variables $\psi^\dagger_{\mathbf{q}},\psi_{-\mathbf{q}}$ and for the particle-hole excitations $\{e^\dagger_{\mathbf{k}+\mathbf{q}}h^\dagger_{-\mathbf{k}}\}$, $\{h_{-\mathbf{k}}e_{\mathbf{k}-\mathbf{q}}\}$, $\{e^\dagger_{\mathbf{k}+\mathbf{q}}e_{-\mathbf{k}}\}$, and $\{h^\dagger_{\mathbf{k}+\mathbf{q}}h_{-\mathbf{k}}\}$ (for all $\mathbf{k}$) would have to be solved. Such a study is left for the future. For now, one might speculate that the influence of Goldstone modes on the spectra is of minor importance since their respective coupling strengths in $A(\mathbf{k},\omega)$ and $B(\mathbf{q},\omega)$ are of higher order in the interaction parameter g.

ACKNOWLEDGMENTS

The authors would like to thank D. Semkat, H. Stolz, and B. Zenker for valuable discussions. This work was funded by Vietnam National Foundation for Science and Technology Development (NAFOSTED) under Grant No. 103.01-2014.05 and by Deutsche Forschungsgemeinschaft (Germany) through the Collaborative Research Center 652, Projects No. B5 and No. B14.

APPENDIX A: MEAN-FIELD APPROXIMATION

The mean-field approximation is obtained by neglecting the fluctuation part $\mathcal{H}_1$ in Eq. (12), i.e., the Hamiltonian reduces to

$$\mathcal{H}_{\rm MF}=\sum_{\mathbf{k}}\hat{\varepsilon}^e_{\mathbf{k}}e^\dagger_{\mathbf{k}}e_{\mathbf{k}}+\sum_{\mathbf{k}}\hat{\varepsilon}^h_{\mathbf{k}}h^\dagger_{\mathbf{k}}h_{\mathbf{k}}+\sum_{\mathbf{q}}\omega_{\mathbf{q}}\Psi^\dagger_{\mathbf{q}}\Psi_{\mathbf{q}}+\Delta\sum_{\mathbf{k}}(e^\dagger_{\mathbf{k}}h^\dagger_{-\mathbf{k}}+\text{H.c.}). \tag{A1}$$

Here, $\hat{\varepsilon}^e_{\mathbf{k}}$, $\hat{\varepsilon}^h_{\mathbf{k}},\Delta$, and $\Psi^\dagger_{\mathbf{q}}$ are given by Eqs. (15), (17), (19), and (22). The electronic part of $\mathcal{H}_{\rm MF}$ is easily diagonalized. By introducing

$$C^\dagger_{1\mathbf{k}}=\xi_{\mathbf{k}}e^\dagger_{\mathbf{k}}+\eta_{\mathbf{k}}h_{-\mathbf{k}}, \tag{A2}$$

$$C^\dagger_{2\mathbf{k}}=-\eta_{\mathbf{k}}e^\dagger_{\mathbf{k}}+\xi_{\mathbf{k}}h_{-\mathbf{k}}, \tag{A3}$$

with ($\xi_{\mathbf{k}},\eta_{\mathbf{k}}$ real)

$$\xi^2_{\mathbf{k}}=\frac{1}{2}\left[1+\text{sgn}\big(\hat{\varepsilon}^e_{\mathbf{k}}+\hat{\varepsilon}^h_{\mathbf{k}}\big)\frac{\hat{\varepsilon}^e_{\mathbf{k}}+\hat{\varepsilon}^h_{\mathbf{k}}}{W_{\mathbf{k}}}\right], \tag{A4}$$

$$\eta^2_{\mathbf{k}}=\frac{1}{2}\left[1-\text{sgn}\big(\hat{\varepsilon}^e_{\mathbf{k}}+\hat{\varepsilon}^h_{\mathbf{k}}\big)\frac{\hat{\varepsilon}^e_{\mathbf{k}}+\hat{\varepsilon}^h_{\mathbf{k}}}{W_{\mathbf{k}}}\right], \tag{A5}$$

$$W_{\mathbf{k}}=\sqrt{\big(\hat{\varepsilon}^e_{\mathbf{k}}+\hat{\varepsilon}^h_{\mathbf{k}}\big)^2+4|\Delta|^2}, \tag{A6}$$

one arrives at

$$\mathcal{H}_{\rm MF}=\sum_{\mathbf{k}}E^1_{\mathbf{k}}C^\dagger_{1\mathbf{k}}C_{1\mathbf{k}}+\sum_{\mathbf{k}}E^2_{\mathbf{k}}C^\dagger_{2\mathbf{k}}C_{2\mathbf{k}}+\sum_{\mathbf{q}}\omega_{\mathbf{q}}\Psi^\dagger_{\mathbf{q}}\Psi_{\mathbf{q}}, \tag{A7}$$

with

$$E^{1,2}_{\mathbf{k}}=\frac{\hat{\varepsilon}^e_{\mathbf{k}}-\hat{\varepsilon}^h_{\mathbf{k}}}{2}\pm\text{sgn}\big(\hat{\varepsilon}^e_{\mathbf{k}}+\hat{\varepsilon}^h_{\mathbf{k}}\big)\frac{W_{\mathbf{k}}}{2}. \tag{A8}$$

The diagonal form (A7) allows to evaluate all physical quantities in mean-field approximation. For instance,

$$\langle n^e_{\mathbf{k}}\rangle=|\xi_{\mathbf{k}}|^2f\big(E^1_{\mathbf{k}}\big)+|\eta_{\mathbf{k}}|^2f\big(E^2_{\mathbf{k}}\big), \tag{A9}$$

$$\langle n^h_{\mathbf{k}}\rangle=1-|\eta_{\mathbf{k}}|^2f\big(E^1_{\mathbf{k}}\big)-|\xi_{\mathbf{k}}|^2f\big(E^2_{\mathbf{k}}\big), \tag{A10}$$

$$d_{\mathbf{k}}=\text{sgn}\big(E^1_{\mathbf{k}}-E^2_{\mathbf{k}}\big)\big(f\big(E^1_{\mathbf{k}}\big)-f\big(E^2_{\mathbf{k}}\big)\big)\frac{\Delta}{W_{\mathbf{k}}}, \tag{A11}$$

$$\langle\psi_{\mathbf{q}=0}\rangle=-\frac{\sqrt{N}\Gamma}{\omega_{\mathbf{q}=0}}, \tag{A12}$$

$$\langle\psi^\dagger_{\mathbf{q}}\psi_{\mathbf{q}}\rangle=p(\omega_{\mathbf{q}})+\frac{N\Gamma^2}{\omega^2_{\mathbf{q}=0}}, \tag{A13}$$

where $p(\omega_{\mathbf{q}})$ is the bosonic distribution function. Note that the phase factor $\text{sgn}(E^1_{\mathbf{k}}-E^2_{\mathbf{k}})$ in Eq. (A11) is found by comparing the exact expression for $d_k=\langle e^\dagger_{\mathbf{k}}h^\dagger_{-\mathbf{k}}\rangle$ with the perturbative result of d_k to lowest order in the coupling term $\Delta\sum_{\mathbf{k}}(e^\dagger_{\mathbf{k}}h^\dagger_{-\mathbf{k}}+\text{H.c.})$ of (A1). Equations (A9)–(A13) lead to the mean-field expressions for the order parameters $\Delta=-(g/\sqrt{N})\langle\psi_0\rangle-(U/N)\sum_{\mathbf{k}}d_{\mathbf{k}}$ and $\Gamma=-(g/N)\sum_{\mathbf{k}}d_{\mathbf{k}}$, whereas the total density $n_{\rm exc}$ is given by

$$n_{\rm exc}=\frac{1}{N}\sum_{\mathbf{q}}p(\omega_{\mathbf{q}})+\frac{\Gamma^2}{\omega^2_{\mathbf{q}=0}}+\frac{1}{2N}\sum_{\mathbf{k}}\left[1-\text{sgn}\big(\hat{\varepsilon}^e_{\mathbf{k}}+\hat{\varepsilon}^h_{\mathbf{k}}\big)\times\frac{\hat{\varepsilon}^e_{\mathbf{k}}+\hat{\varepsilon}^h_{\mathbf{k}}}{W_{\mathbf{k}}}\big[f\big(E^1_{\mathbf{k}}\big)-f\big(E^2_{\mathbf{k}}\big)\big]\right]. \tag{A14}$$

It describes a mean-field condensate of coupled photons and exciton polarization, where the term $\Gamma^2/\omega^2_{\mathbf{q}=0}=\langle\psi_0\rangle^2/N$ is the density of photons in the condensate. The luminescence functions, defined in Eqs. (25) and (29), become

$$A(\mathbf{k},\omega) = \frac{1}{N}\sum_{\mathbf{p}} \times \big(|\xi_{\mathbf{k+p}}\eta_{\mathbf{p}}|^2\big[f\big(E^1_{\mathbf{p}}\big) - f\big(E^1_{\mathbf{k+p}}\big)\big]\delta\big(\omega - E^1_{\mathbf{k+p}} + E^1_{\mathbf{p}}\big) + |\eta_{\mathbf{k+p}}\eta_{\mathbf{p}}|^2\big[f\big(E^1_{\mathbf{p}}\big) - f\big(E^2_{\mathbf{k+p}}\big)\big]\delta\big(\omega - E^2_{\mathbf{k+p}} + E^1_{\mathbf{p}}\big) + |\xi_{\mathbf{k+p}}\xi_{\mathbf{p}}|^2\big[f\big(E^2_{\mathbf{p}}\big) - f\big(E^1_{\mathbf{k+p}}\big)\big]\delta\big(\omega - E^1_{\mathbf{k+p}} + E^2_{\mathbf{p}}\big) + |\eta_{\mathbf{k+p}}\xi_{\mathbf{p}}|^2\big[f\big(E^2_{\mathbf{p}}\big) - f\big(E^2_{\mathbf{k+p}}\big)\big]\delta\big(\omega - E^2_{\mathbf{k+p}} + E^2_{\mathbf{p}}\big)\big) \quad \text{(A15)}$$

and

$$B(\mathbf{q},\omega) = \delta(\omega - \omega_{\mathbf{q}}). \quad \text{(A16)}$$

Note the formal similarity of result (A15) to the coherent part $A^{\rm coh}(\mathbf{k},\omega)$ of the PRM expression (C4) for $A(\mathbf{k},\omega)$ in Appendix C. For the cavity photon spectral function $B(\mathbf{q},\omega)$, the mean-field result reduces to a sole δ function, whereas all contributions from fluctuations in the PRM result (C19) are of course missing.

APPENDIX B: PROJECTOR-BASED RENORMALIZATION METHOD: GENERAL CONCEPTS

In this Appendix, we show how the complete Hamiltonian $\mathcal{H}$ can be solved by means of the PRM. So far, the PRM was successfully applied to a number of different models. Prominent examples are the one-dimensional Holstein model [31], the Edwards model [32], or the extended Falicov-Kimball model [26]. The starting point is always a decomposition of the many-particle Hamiltonian $\mathcal{H}$ into an "unperturbed" part $\mathcal{H}_0$ and into a "perturbation" $\mathcal{H}_1$, where the unperturbed part $\mathcal{H}_0$ is solvable [compare Eqs. (22) and (23)]. The perturbation $\mathcal{H}_1$ is responsible for transitions between the eigenstates of $\mathcal{H}_0$ with nonvanishing transition energies $|E_0^n - E_0^m|$. Here, E_0^n and E_0^m denote the energies of $\mathcal{H}_0$ between which the transitions take place. The basic idea of the PRM method is to integrate out the interaction $\mathcal{H}_1$ by a sequence of discrete unitary transformations [25]. Thereby, the PRM procedure starts from the largest transition energy of the original Hamiltonian $\mathcal{H}_0$, which will be called Λ, and proceeds in small steps $\Delta\lambda$ to lower values of the transition energy λ. Every step is performed by means of a small unitary transformation, where all excitations between λ and $\lambda - \Delta\lambda$ are eliminated:

$$\mathcal{H}_{\lambda-\Delta\lambda} = e^{X_{\lambda,\Delta\lambda}}\,\mathcal{H}_\lambda\, e^{-X_{\lambda,\Delta\lambda}}. \quad \text{(B1)}$$

Here, the operator $X_{\lambda,\Delta\lambda} = -X^\dagger_{\lambda,\Delta\lambda}$ is the generator of the unitary transformation. Note that for sufficiently small $\Delta\lambda$, the evaluation of transformation (B1) can be restricted to low orders in $\mathcal{H}_1$ which usually limits the validity of the approach to values of $\mathcal{H}_1$ of the same magnitude as those of $\mathcal{H}_0$. After each step, the unperturbed part as well as the perturbation part of the Hamiltonian become renormalized and thus depend on the cutoff λ. One arrives at a renormalized Hamiltonian $\mathcal{H}_\lambda = \mathcal{H}_{0,\lambda} + \mathcal{H}_{1,\lambda}$, where $\mathcal{H}_{1,\lambda}$ now only accounts for transitions with energies smaller than λ. Proceeding the renormalization stepwise up to zero transition energy $\lambda = 0$ all transitions with energies different from zero have been integrated out. Thus, one finally arrives at a renormalized Hamiltonian $\mathcal{H}_{\lambda=0}$, which is diagonal (or at least quasidiagonal) since all transitions from $\mathcal{H}_1$ with nonzero energies have been used up.

1. Hamiltonian $\mathcal{H}_\lambda$

Let us assume that all transitions with energies larger than λ have already been integrated out. An appropriate ansatz for the transformed Hamiltonian $\mathcal{H}_\lambda$ reads as $\mathcal{H}_\lambda = \mathcal{H}_{0,\lambda} + \mathcal{H}_{1,\lambda}$ with

$$\mathcal{H}_{0,\lambda} = \sum_{\mathbf{k}} \varepsilon^e_{\mathbf{k},\lambda} e^\dagger_{\mathbf{k}} e_{\mathbf{k}} + \sum_{\mathbf{k}} \varepsilon^h_{\mathbf{k},\lambda} h^\dagger_{\mathbf{k}} h_{\mathbf{k}} + \sum_{\mathbf{k}} \Delta_{\mathbf{k},\lambda}(e^\dagger_{\mathbf{k}} h^\dagger_{-\mathbf{k}} + \text{H.c.}) + \sum_{\mathbf{p}} \omega_{\mathbf{q},\lambda} \Psi^\dagger_{\mathbf{q},\lambda}\Psi_{\mathbf{q},\lambda}, \quad \text{(B2)}$$

$$\mathcal{H}_{1,\lambda} = -\frac{g}{\sqrt{N}} \sum_{\mathbf{kq}} \mathbf{P}_\lambda[:\, e^\dagger_{\mathbf{k+q}} h^\dagger_{-\mathbf{k}} \Psi_{\mathbf{q},\lambda} : + \text{H.c.}] - \frac{U}{N} \sum_{\mathbf{k}_1\mathbf{k}_2\mathbf{k}_3} \mathbf{P}_\lambda\big[\, : e^\dagger_{\mathbf{k}_1} e_{\mathbf{k}_2} h^\dagger_{\mathbf{k}_3} h_{\mathbf{k}_1+\mathbf{k}_3-\mathbf{k}_2} : \big]. \quad \text{(B3)}$$

Clearly, all parameters of $\mathcal{H}_{0,\lambda}$ now depend on the cutoff λ, and $\Delta_{\mathbf{k},\lambda}$ has acquired an additional momentum dependence. Moreover, we have introduced a λ-dependent photon operator

$$\Psi^\dagger_{\mathbf{q},\lambda} = \psi^\dagger_{\mathbf{q}} + \frac{\sqrt{N}\Gamma_\lambda}{\omega_{\mathbf{q}=\mathbf{0},\lambda}} \delta_{\mathbf{q},\mathbf{0}},, \quad \text{(B4)}$$

which is a slight generalization of the former definition (21). Finally, the quantity $\mathbf{P}_\lambda$ in Eq. (B3) is a generalized projector, which projects on all transitions with energies smaller than λ (with respect to $\mathcal{H}_{0,\lambda}$). Note that the coupling strength g of $\mathcal{H}_{1,\lambda}$ remains λ independent, which is a consequence of the present restriction to renormalization contributions up to order g^2 and U^2.

Next, $\mathbf{P}_\lambda$ has to be applied to the operators in $\mathcal{H}_{1,\lambda}$, which requires the decomposition of the operators in the squared brackets into dynamical eigenmodes of $\mathcal{H}_{0,\lambda}$. As long as one is only interested in renormalization equations up to linear order in the order parameters, one finds

$$\mathcal{H}_{1,\lambda} = -\frac{g}{\sqrt{N}} \sum_{\mathbf{kq}} \Theta_{\mathbf{kq},\lambda}[:\, e^\dagger_{\mathbf{k+q}} h^\dagger_{-\mathbf{k}} \Psi_{\mathbf{q},\lambda} : + \text{H.c.}] - \frac{U}{N} \sum_{\mathbf{k}_1\mathbf{k}_2\mathbf{k}_3} \Theta_{\mathbf{k}_1\mathbf{k}_2\mathbf{k}_3,\lambda} : e^\dagger_{\mathbf{k}_1} e_{\mathbf{k}_2} h^\dagger_{\mathbf{k}_3} h_{\mathbf{k}_1+\mathbf{k}_3-\mathbf{k}_2} : , \quad \text{(B5)}$$

where we have introduced two Θ functions

$$\Theta_{\mathbf{kq},\lambda} = \Theta\big(\lambda - \big|\varepsilon^e_{\mathbf{k+q},\lambda} + \varepsilon^h_{-\mathbf{k},\lambda} - \omega_{\mathbf{q},\lambda}\big|\big), \quad \text{(B6)}$$

$$\Theta_{\mathbf{k}_1\mathbf{k}_2\mathbf{k}_3,\lambda} = \Theta\big(\lambda - \big|\varepsilon^e_{\mathbf{k}_1,\lambda} - \varepsilon^e_{\mathbf{k}_2,\lambda} + \varepsilon^h_{\mathbf{k}_3,\lambda} - \varepsilon^h_{\mathbf{k}_1+\mathbf{k}_3-\mathbf{k}_2,\lambda}\big|\big). \quad \text{(B7)}$$

They restrict transitions to excitation energies smaller than λ. Next, one constructs the generator $X_{\lambda,\Delta\lambda}$ of the unitary transformation (B1). According to Ref. [25], the lowest order for $X_{\lambda,\Delta\lambda}$ is given by

$$X_{\lambda,\Delta\lambda} = \frac{1}{\mathbf{L}_{0,\lambda}} \mathbf{Q}_{\lambda-\Delta\lambda}\mathcal{H}_{1,\lambda}, \quad \text{(B8)}$$

where $\mathbf{L}_{0,\lambda}$ is the Liouville operator of the unperturbed Hamiltonian $\mathcal{H}_{0,\lambda}$. It is defined by $\mathbf{L}_{0,\lambda}\mathcal{A} = [\mathcal{H}_{0,\lambda},\mathcal{A}]$ for any operator quantity $\mathcal{A}$, and $\mathbf{Q}_{\lambda-\Delta\lambda} = 1 - \mathbf{P}_{\lambda-\Delta\lambda}$ is the complement projector to $\mathbf{P}_{\lambda-\Delta\lambda}$, i.e., $\mathbf{Q}_{\lambda-\Delta\lambda}$ projects on all transitions with energies larger than $\lambda - \Delta\lambda$. With Eqs. (B5) and (B2) one finds

$$X_{\lambda,\Delta\lambda} = -\frac{g}{\sqrt{N}}\sum_{\mathbf{kq}} A_{\mathbf{kq}}(\lambda,\Delta\lambda)[: e^{\dagger}_{\mathbf{k+q}}h^{\dagger}_{-\mathbf{k}}\Psi_{\mathbf{q},\lambda} : - \text{H.c.}] - \frac{U}{N}\sum_{\mathbf{k}_1\mathbf{k}_2\mathbf{k}_3} B_{\mathbf{k}_1\mathbf{k}_2\mathbf{k}_3}(\lambda,\Delta\lambda) : e^{\dagger}_{\mathbf{k}_1}e_{\mathbf{k}_2}h^{\dagger}_{\mathbf{k}_3}h_{\mathbf{k}_1+\mathbf{k}_3-\mathbf{k}_2} : \tag{B9}$$

with the definitions

$$A_{\mathbf{kq}}(\lambda,\Delta\lambda) = \frac{\Theta_{\mathbf{kq},\lambda}(1-\Theta_{\mathbf{kq},\lambda-\Delta\lambda})}{\varepsilon^{e}_{\mathbf{k+q},\lambda} + \varepsilon^{h}_{-\mathbf{k},\lambda} - \omega_{\mathbf{q},\lambda}}, \tag{B10}$$

$$B_{\mathbf{k}_1\mathbf{k}_2\mathbf{k}_3}(\lambda,\Delta\lambda) = \frac{\Theta_{\mathbf{k}_1\mathbf{k}_2\mathbf{k}_3,\lambda}\left(1-\Theta_{\mathbf{k}_1\mathbf{k}_2\mathbf{k}_3,\lambda-\Delta\lambda}\right)}{\varepsilon^{e}_{\mathbf{k}_1,\lambda} - \varepsilon^{e}_{\mathbf{k}_2,\lambda} + \varepsilon^{h}_{\mathbf{k}_3,\lambda} - \varepsilon^{h}_{\mathbf{k}_1+\mathbf{k}_3-\mathbf{k}_2,\lambda}}. \tag{B11}$$

Here, the products of the two Θ functions in $A_{\mathbf{kq}}(\lambda,\Delta\lambda)$ and $B_{\mathbf{k}_1\mathbf{k}_2\mathbf{k}_3}(\lambda,\Delta\lambda)$ assure that only excitations between λ and $\lambda-\Delta\lambda$ are eliminated by the unitary transformation (B1). In principle, the Liouville operator $\mathbf{L}_{0,\lambda}$ in $X_{\lambda,\Delta\lambda}$ (and the projector $\mathbf{P}_{\lambda}$ in $\mathcal{H}_{1,\lambda}$) should have been defined with the full unperturbed Hamiltonian $\mathcal{H}_{0,\lambda}$ of Eq. (B2) and not by leaving out the term $\propto\Delta_{\mathbf{k},\lambda}$. However, its inclusion would only give rise to smaller higher-order corrections to $\Delta_{\mathbf{k},\lambda}$ and is not important.

2. Renormalization equations

The λ dependence of the parameters of $\mathcal{H}_{\lambda}$ is found from transformation (B1). For small enough width $\Delta\lambda$ of the transformation steps, an expansion of (B1) in g and U can be limited to $O(g^2)$ and $O(U^2)$ terms. One obtains

$$\mathcal{H}_{\lambda-\Delta\lambda} = \mathcal{H}_{0,\lambda} + \mathbf{P}_{\lambda-\Delta\lambda}\mathcal{H}_{1,\lambda} + [X_{\lambda,\Delta\lambda},\mathcal{H}_{1,\lambda}] - \tfrac{1}{2}[X_{\lambda,\Delta\lambda},\mathbf{Q}_{\lambda-\Delta\lambda}\mathcal{H}_{1,\lambda}] + \cdots, \tag{B12}$$

where Eq. (B8) has been used. Renormalization contributions to $\mathcal{H}_{\lambda-\Delta\lambda}$ arise from the last two commutators which have to be evaluated explicitly. The result must be compared with the generic forms (B2) and (B5) of $\mathcal{H}_{\lambda}$ (with λ replaced by $\lambda-\Delta\lambda$) when it is written in terms of the original λ-independent variables $e^{\dagger}_{\mathbf{k}}$, $h^{\dagger}_{\mathbf{k}}$, and $\psi^{\dagger}_{\mathbf{q}}$. This leads to the following renormalization equations for the parameters of $\mathcal{H}_{0,\lambda}$:

$$\varepsilon^{e}_{\mathbf{k},\lambda-\Delta\lambda} = \varepsilon^{e}_{\mathbf{k},\lambda} + \frac{2g^2}{N}\sum_{\mathbf{q}} A_{\mathbf{q},\mathbf{k-q}}(\lambda,\Delta\lambda)\left(n^{\Psi}_{\mathbf{q}} + n^{h}_{\mathbf{q-k}}\right) + \frac{U^2}{N^2}\sum_{\mathbf{k}_1\mathbf{k}_2} B_{\mathbf{k}_1\mathbf{k}\mathbf{k}_2}(\lambda,\Delta\lambda)\left(1-2n^{e}_{\mathbf{k}_1}\right)\left(n^{h}_{\mathbf{k}_2} - n^{h}_{\mathbf{k}_1+\mathbf{k}_2-\mathbf{k}}\right) + \frac{U^2}{N^2}\sum_{\mathbf{k}_1\mathbf{k}_2} B_{\mathbf{k},\mathbf{k}+\mathbf{k}_1-\mathbf{k}_2,\mathbf{k}_1}(\lambda,\Delta\lambda)\left[n^{h}_{\mathbf{k}_2}\left(1-n^{h}_{\mathbf{k}_1}\right) + n^{h}_{\mathbf{k}_1}\left(1-n^{h}_{\mathbf{k}_2}\right)\right], \tag{B13}$$

$$\varepsilon^{h}_{\mathbf{k},\lambda-\Delta\lambda} = \varepsilon^{h}_{\mathbf{k},\lambda} + \frac{2g^2}{N}\sum_{\mathbf{q}} A_{\mathbf{q},-\mathbf{k}}(\lambda,\Delta\lambda)\left(n^{\Psi}_{\mathbf{q}} + n^{e}_{\mathbf{q-k}}\right) + \frac{U^2}{N^2}\sum_{\mathbf{k}_1\mathbf{k}_2} B_{\mathbf{k}_1,\mathbf{k}_1+\mathbf{k}_2-\mathbf{k},\mathbf{k}_2}(\lambda,\Delta\lambda)\left(1-2n^{h}_{\mathbf{k}_2}\right)\left(n^{e}_{\mathbf{k}_1} - n^{e}_{\mathbf{k}_1+\mathbf{k}_2-\mathbf{k}}\right) + \frac{U^2}{N^2}\sum_{\mathbf{k}_1\mathbf{k}_2} B_{\mathbf{k}_1\mathbf{k}_2\mathbf{k}}(\lambda,\Delta\lambda)\left[n^{e}_{\mathbf{k}_2}\left(1-n^{e}_{\mathbf{k}_1}\right) + n^{e}_{\mathbf{k}_1}\left(1-n^{e}_{\mathbf{k}_2}\right)\right], \tag{B14}$$

and

$$\omega_{\mathbf{k},\lambda-\Delta\lambda} = \omega_{\mathbf{k},\lambda} + \frac{2g^2}{N}\sum_{\mathbf{q}} A_{\mathbf{k},\mathbf{q}}(\lambda,\Delta\lambda)\left(n^{e}_{\mathbf{q+k}} + n^{h}_{-\mathbf{q}} - 1\right), \tag{B15}$$

$$\Gamma_{\lambda-\Delta\lambda} = \Gamma_{\lambda} - \frac{2g^2}{N\sqrt{N}}\sum_{\mathbf{q}} A_{\mathbf{0},\mathbf{q}}(\lambda,\Delta\lambda)\langle\psi_0\rangle\left(n^{e}_{\mathbf{q}} + n^{h}_{-\mathbf{q}} - 1\right), \tag{B16}$$

$$\Delta_{\mathbf{k},\lambda-\Delta\lambda} = \Delta_{\mathbf{k},\lambda} - \frac{U^2}{N^2}\sum_{\mathbf{k}_1\mathbf{k}_2}\left[\Gamma^{\mathbf{k}_1\mathbf{k},-\mathbf{k}_2}_{\mathbf{k}_1\mathbf{k}_2,-\mathbf{k}}(\lambda,\Delta\lambda) + \Gamma^{\mathbf{k}_1\mathbf{k},-\mathbf{k}_1}_{\mathbf{k}_1\mathbf{k}_2,-\mathbf{k}_1}(\lambda,\Delta\lambda)\right]\left(2n^{e}_{\mathbf{k}_1}-1\right)d_{\mathbf{k}_2} - \frac{U^2}{N^2}\sum_{\mathbf{k}_1\mathbf{k}_2}\left[\Gamma^{\mathbf{k}_2,\mathbf{k}_1+\mathbf{k}_2+\mathbf{k},\mathbf{k}_1}_{\mathbf{k},\mathbf{k}_1+\mathbf{k}_2+\mathbf{k},\mathbf{k}_1}(\lambda,\Delta\lambda) + \Gamma^{\mathbf{k}_2,-\mathbf{k}_1,-\mathbf{k}_2}_{\mathbf{k},-\mathbf{k}_1,-\mathbf{k}}(\lambda,\Delta\lambda)\right]\left(2n^{h}_{\mathbf{k}_1}-1\right)d_{\mathbf{k}_2} + \frac{2U^2}{N^2}\sum_{\mathbf{k}_1\mathbf{k}_2}\Gamma^{\mathbf{k}_1 k_2,-\mathbf{k}_1}_{\mathbf{k}_1\mathbf{k},-\mathbf{k}_1}(\lambda,\Delta\lambda)\left(1-n^{e}_{\mathbf{k}_1}-n^{h}_{-\mathbf{k}_1}\right)d_{\mathbf{k}_2} - \frac{U}{N}\sum_{\mathbf{k}_1} B_{\mathbf{k}\mathbf{k}_1,-\mathbf{k}}(\lambda,\Delta\lambda)\Delta_{\mathbf{k}_1,\lambda}\left(1-n^{h}_{-\mathbf{k}_1}-n^{e}_{\mathbf{k}_1}\right). \tag{B17}$$

The quantities $n^{e}_{\mathbf{k}}$ and $n^{h}_{\mathbf{k}}$ are the occupation numbers for electrons and holes from Eq. (17), and $d_{\mathbf{k}}$ was defined in Eq. (20). Following, we shall also use the photonic occupation number $n^{\Psi}_{\mathbf{q},\lambda}$,

$$n^{\Psi}_{\mathbf{q},\lambda} = \langle\delta\Psi^{\dagger}_{\mathbf{q},\lambda}\delta\Psi_{\mathbf{q},\lambda}\rangle = \langle\Psi^{\dagger}_{\mathbf{q},\lambda}\Psi_{\mathbf{q},\lambda}\rangle - \langle\Psi^{\dagger}_{\mathbf{q},\lambda}\rangle\langle\Psi_{\mathbf{q},\lambda}\rangle = \langle\delta\psi^{\dagger}_{\mathbf{q}}\delta\psi_{\mathbf{q}}\rangle = n^{\psi}_{\mathbf{q}}, \tag{B18}$$

which is independent of λ. In Eq. (B17), we have also defined

$$\Gamma^{\mathbf{k}_1\mathbf{k}_2\mathbf{k}_3}_{\mathbf{k}_1'\mathbf{k}_2'\mathbf{k}_3'}(\lambda,\Delta\lambda) = \tfrac{1}{2}\big[B_{\mathbf{k}_1'\mathbf{k}_2'\mathbf{k}_3'}(\lambda,\Delta\lambda)\,\Theta_{\mathbf{k}_1\mathbf{k}_2\mathbf{k}_3,\lambda} + B_{\mathbf{k}_1\mathbf{k}_2\mathbf{k}_3}(\lambda,\Delta\lambda)\,\Theta_{\mathbf{k}_1'\mathbf{k}_2'\mathbf{k}_3',\lambda}\big]. \quad \text{(B19)}$$

For the numerical solution of the renormalization equations, the initial parameter values are those of the original model $\mathcal{H}$ ($\lambda = \Lambda$):

$$\varepsilon^e_{\mathbf{k},\Lambda} = \hat{\varepsilon}^e_{\mathbf{k}}, \quad \varepsilon^h_{\mathbf{k},\Lambda} = \hat{\varepsilon}^h_{\mathbf{k}}, \quad \omega_{\mathbf{k},\Lambda} = \omega_{\mathbf{k}} \quad \text{(B20)}$$

and

$$\Delta_{\mathbf{k},\Lambda} = \Delta = -\frac{g}{\sqrt{N}}\langle\psi_0\rangle - \frac{U}{N}\sum_{\mathbf{k}} d_{\mathbf{k}}, \quad \text{(B21)}$$

$$\Gamma_\Lambda = \Gamma = -\frac{g}{N}\sum_{\mathbf{k}} d_{\mathbf{k}}, \quad \text{(B22)}$$

with $\langle\psi_0\rangle = 0^+$, $d_{\mathbf{k}} = \langle e^\dagger_{\mathbf{k}} h^\dagger_{-\mathbf{k}}\rangle = 0^+$. Suppose the expectation values in Eqs. (B13)–(B17) would already be known, the renormalization equations can be integrated between $\lambda = \Lambda$ and 0. In this way, we obtain the fully renormalized Hamiltonian $\tilde{\mathcal{H}} := \mathcal{H}_{\lambda=0} = \mathcal{H}_{0,\lambda=0}$, as was already stated in Eq. (24):

$$\tilde{\mathcal{H}} = \sum_{\mathbf{k}} \tilde{\varepsilon}^e_{\mathbf{k}} e^\dagger_{\mathbf{k}} e_{\mathbf{k}} + \sum_{\mathbf{k}} \tilde{\varepsilon}^h_{\mathbf{k}} h^\dagger_{\mathbf{k}} h_{\mathbf{k}} + \sum_{\mathbf{k}} \tilde{\Delta}_{\mathbf{k}}(e^\dagger_{\mathbf{k}} h^\dagger_{-\mathbf{k}} + \text{H.c.}) + \sum_{\mathbf{q}} \tilde{\omega}_{\mathbf{q}} \tilde{\Psi}^\dagger_{\mathbf{q}} \tilde{\Psi}_{\mathbf{q}}. \quad \text{(B23)}$$

The tilde symbols denote the fully renormalized quantities at $\lambda = 0$ as before. All excitations from $\mathcal{H}_{1,\lambda}$ with nonzero energies have been eliminated. They give rise to the renormalization of $\mathcal{H}_{0,\lambda}$.

Finally, the electronic part of $\tilde{\mathcal{H}}$ will be diagonalized by a Bogoliubov transformation in close analogy to Appendix A. Defining again new linear combinations

$$C^\dagger_{1\mathbf{k}} = \xi_{\mathbf{k}} e^\dagger_{\mathbf{k}} + \eta_{\mathbf{k}} h_{-\mathbf{k}}, \quad \text{(B24)}$$

$$C^\dagger_{2\mathbf{k}} = -\eta_{\mathbf{k}} e^\dagger_{\mathbf{k}} + \xi_{\mathbf{k}} h_{-\mathbf{k}} \quad \text{(B25)}$$

(with $\eta_{\mathbf{k}},\xi_{\mathbf{k}}$ assumed to be real), where now the renormalized one-particles energies $\tilde{\varepsilon}^e_{\mathbf{k}}$ and $\tilde{\varepsilon}^h_{\mathbf{k}}$ enter the prefactors $\xi_{\mathbf{k}}$ and $\eta_{\mathbf{k}}$,

$$\xi^2_{\mathbf{k}} = \frac{1}{2}\left[1 + \text{sgn}\big(\tilde{\varepsilon}^e_{\mathbf{k}} + \tilde{\varepsilon}^h_{\mathbf{k}}\big)\frac{\tilde{\varepsilon}^e_{\mathbf{k}} + \tilde{\varepsilon}^h_{\mathbf{k}}}{W_{\mathbf{k}}}\right], \quad \text{(B26)}$$

$$\eta^2_{\mathbf{k}} = \frac{1}{2}\left[1 - \text{sgn}\big(\tilde{\varepsilon}^e_{\mathbf{k}} + \tilde{\varepsilon}^h_{\mathbf{k}}\big)\frac{\tilde{\varepsilon}^e_{\mathbf{k}} + \tilde{\varepsilon}^h_{\mathbf{k}}}{W_{\mathbf{k}}}\right], \quad \text{(B27)}$$

$$W_{\mathbf{k}} = \sqrt{\big(\tilde{\varepsilon}^e_{\mathbf{k}} + \tilde{\varepsilon}^h_{\mathbf{k}}\big)^2 + 4|\tilde{\Delta}_{\mathbf{k}}|^2}, \quad \text{(B28)}$$

one finds

$$\tilde{\mathcal{H}} = \sum_{\mathbf{k}} \tilde{E}^1_{\mathbf{k}} C^\dagger_{1\mathbf{k}} C_{1\mathbf{k}} + \sum_{\mathbf{k}} \tilde{E}^2_{\mathbf{k}} C^\dagger_{2\mathbf{k}} C_{2\mathbf{k}} + \sum_{\mathbf{q}} \tilde{\omega}_{\mathbf{q}} \tilde{\Psi}^\dagger_{\mathbf{q}} \tilde{\Psi}_{\mathbf{q}}, \quad \text{(B29)}$$

with

$$\tilde{E}^{1,2}_{\mathbf{k}} = \frac{\tilde{\varepsilon}^e_{\mathbf{k}} - \tilde{\varepsilon}^h_{\mathbf{k}}}{2} \pm \text{sgn}\big(\tilde{\varepsilon}^e_{\mathbf{k}} + \tilde{\varepsilon}^h_{\mathbf{k}}\big)\frac{W_{\mathbf{k}}}{2}. \quad \text{(B30)}$$

Here, the electronic quasiparticle energies $\tilde{E}^{(1,2)}_{\mathbf{k}}$ and the quasiparticle modes $C^{(\dagger)}_{1\mathbf{k}},C^{(\dagger)}_{2\mathbf{k}}$ are renormalized quantities as well. The quadratic form of Eq. (B29) allows to compute any expectation value formed with $\tilde{\mathcal{H}}$. Finally, we note that the diagonalization (B24) runs along the same lines as the former Bogoliubov transformation of expression (22) for $\mathcal{H}_0$, except that the renormalized quantities have to be replaced by the unrenormalized ones.

3. Expectation values

Also, expectation values $\langle\mathcal{A}\rangle$, formed with the full $\mathcal{H}$, can be evaluated in the framework of the PRM. As already stated in Sec. III, they are found by exploiting the unitary invariance of operator expressions below a trace, $\langle\mathcal{A}\rangle = \langle\mathcal{A}(\lambda)\rangle_{\mathcal{H}_\lambda} = \langle\tilde{\mathcal{A}}\rangle_{\tilde{\mathcal{H}}}$, where $\mathcal{A}(\lambda) = e^{X_\lambda}\mathcal{A}e^{-X_\lambda}$ and $\tilde{\mathcal{A}} = \mathcal{A}(\lambda = 0)$. X_λ is the generator for the unitary transformation between cutoff Λ and λ. To find the expectation values of Eqs. (B13)–(B17), one best starts from an appropriate ansatz for the single-fermion operators

$$e^\dagger_{\mathbf{k}}(\lambda) = x_{\mathbf{k},\lambda} e^\dagger_{\mathbf{k}} + \frac{1}{\sqrt{N}}\sum_{\mathbf{q}} t_{\mathbf{k}-\mathbf{q},\mathbf{q},\lambda} h_{-\mathbf{q}} : \Psi^\dagger_{\mathbf{k}-\mathbf{q},\lambda} : + \frac{1}{N}\sum_{\mathbf{k}_1\mathbf{k}_2} \alpha_{\mathbf{k}_1\mathbf{k}\mathbf{k}_2,\lambda} : e^\dagger_{\mathbf{k}_1} h^\dagger_{\mathbf{k}_2} h_{\mathbf{k}_1+\mathbf{k}_2-\mathbf{k}} :, \quad \text{(B31)}$$

$$h^\dagger_{\mathbf{k}}(\lambda) = y_{\mathbf{k},\lambda} h^\dagger_{\mathbf{k}} + \frac{1}{\sqrt{N}}\sum_{\mathbf{q}} u_{\mathbf{q},-\mathbf{k},\lambda} e_{\mathbf{q}-\mathbf{k}} : \Psi^\dagger_{\mathbf{q},\lambda} : + \frac{1}{N}\sum_{\mathbf{k}_1\mathbf{k}_2} \beta_{\mathbf{k}_1\mathbf{k}_2,\mathbf{k}-\mathbf{k}_1+\mathbf{k}_2,\lambda} : e^\dagger_{\mathbf{k}_1} e_{\mathbf{k}_2} h^\dagger_{\mathbf{k}-\mathbf{k}_1+\mathbf{k}_2} : \quad \text{(B32)}$$

(where $: \Psi^\dagger_{\mathbf{k},\lambda} :=: \psi^\dagger_{\mathbf{k}} :$), and for the photon operator

$$\psi^\dagger_{\mathbf{q}}(\lambda) = z_{\mathbf{q},\lambda}\psi^\dagger_{\mathbf{q}} + \frac{1}{\sqrt{N}}\sum_{\mathbf{k}} v_{\mathbf{q}\mathbf{k},\lambda} : e^\dagger_{\mathbf{k}+\mathbf{q}} h^\dagger_{-\mathbf{k}} :, \quad \text{(B33)}$$

where again the operator structures of (B31)–(B33) were taken over from a small-X_λ expansion. In analogy to the renormalization equations for the parameters of $\mathcal{H}_\lambda$, one derives the following set of renormalization equations for the λ-dependent coefficients $t_{\mathbf{k}-\mathbf{q},\mathbf{q},\lambda}$, $u_{\mathbf{q},-\mathbf{k},\lambda}$, $v_{\mathbf{k},\mathbf{q},\lambda}$, $\alpha_{\mathbf{k}_1\mathbf{k}_2\mathbf{k}_3,\lambda}$, and $\beta_{\mathbf{k}_1\mathbf{k}_2\mathbf{k}_3,\lambda}$:

$$t_{\mathbf{k}-\mathbf{q},\mathbf{q},\lambda-\Delta\lambda} = t_{\mathbf{k}-\mathbf{q},\mathbf{q},\lambda} + g x_{\mathbf{k},\lambda} A_{\mathbf{k}-\mathbf{q},\mathbf{q}}(\lambda,\Delta\lambda), \quad \text{(B34)}$$

$$u_{\mathbf{q},-\mathbf{k},\lambda-\Delta\lambda} = u_{\mathbf{q},-\mathbf{k},\lambda} - g y_{\mathbf{k},\lambda} A_{\mathbf{q},-\mathbf{k}}(\lambda,\Delta\lambda), \quad \text{(B35)}$$

$$v_{\mathbf{k}\mathbf{q},\lambda-\Delta\lambda} = v_{\mathbf{k}\mathbf{q},\lambda} - g z_{\mathbf{k},\lambda} A_{\mathbf{k}\mathbf{q}}(\lambda,\Delta\lambda), \quad \text{(B36)}$$

$$\alpha_{\mathbf{k}_1\mathbf{k}\mathbf{k}_2,\lambda-\Delta\lambda} = \alpha_{\mathbf{k}_1\mathbf{k}\mathbf{k}_2,\lambda} - U x_{\mathbf{k},\lambda} B_{\mathbf{k}_1\mathbf{k}\mathbf{k}_2}(\lambda,\Delta\lambda), \quad \text{(B37)}$$

$$\beta_{\mathbf{k}_1\mathbf{k}_2,\mathbf{k}-\mathbf{k}_1+\mathbf{k}_2,\lambda-\Delta\lambda} = \beta_{\mathbf{k}_1\mathbf{k}_2,\mathbf{k}-\mathbf{k}_1+\mathbf{k}_2,\lambda} - U y_{\mathbf{k},\lambda} B_{\mathbf{k}_1\mathbf{k}_2,\mathbf{k}-\mathbf{k}_1+\mathbf{k}_2}(\lambda,\Delta\lambda). \quad \text{(B38)}$$

Using the anticommutation relations for fermion operators and the commutation relations for boson operators (as for instance

$[e^\dagger_{\mathbf{k}}(\lambda),e_{\mathbf{k}}(\lambda)]_+ = 1$, valid for any λ), one arrives at

$$|x_{\mathbf{k},\lambda}|^2 = 1 - \frac{1}{N}\sum_{\mathbf{q}} |t_{\mathbf{k-q,q},\lambda}|^2\big(n^{\Psi}_{\mathbf{k-q},\lambda} + n^h_{-\mathbf{q}}\big) - \frac{1}{N^2}\sum_{\mathbf{k}_1\mathbf{k}_2}\big|\alpha_{\mathbf{k}_1\mathbf{k}\mathbf{k}_2,\lambda}\big|^2\big[n^h_{\mathbf{k}_1+\mathbf{k}_2-\mathbf{k}}\big(1-n^h_{\mathbf{k}_2}\big) - n^e_{\mathbf{k}_1}\big(n^h_{\mathbf{k}_1+\mathbf{k}_2-\mathbf{k}} - n^h_{\mathbf{k}_2}\big)\big], \tag{B39}$$

$$|y_{\mathbf{k},\lambda}|^2 = 1 - \frac{1}{N}\sum_{\mathbf{q}} |u_{\mathbf{q},-\mathbf{k},\lambda}|^2\big(n^{\Psi}_{\mathbf{q},\lambda} + n^e_{\mathbf{q-k}}\big) - \frac{1}{N^2}\sum_{\mathbf{k}_1\mathbf{k}_2}\big|\beta_{\mathbf{k}_1\mathbf{k}_2,\mathbf{k}-\mathbf{k}_1+\mathbf{k}_2,\lambda}\big|^2\big[n^e_{\mathbf{k}_1}\big(1-n^e_{\mathbf{k}_2}\big) + \big(1-n^h_{\mathbf{k}-\mathbf{k}_1+\mathbf{k}_2}\big(n^e_{\mathbf{k}_2} - n^e_{\mathbf{k}_1}\big)\big], \tag{B40}$$

$$|z_{\mathbf{k},\lambda}|^2 = 1 - \frac{1}{N}\sum_{\mathbf{q}} |v_{\mathbf{qk},\lambda}|^2\big(1 - n^h_{-\mathbf{k}} - n^e_{\mathbf{k+q}}\big). \tag{B41}$$

Equations (B34)–(B38) together with the new set (B39)–(B41), taken at $\lambda \to \lambda - \Delta\lambda$, represent a complete set of renormalization equations for all λ-dependent coefficients in Eqs. (B31)–(B33). They combine the parameter values at λ with those at $\lambda - \Delta\lambda$. Their initial values at $\lambda = \Lambda$ are

$$\{x_{\mathbf{k},\Lambda}, y_{\mathbf{k},\Lambda}, z_{\mathbf{k},\Lambda}\} = 1, \tag{B42}$$

$$\{t_{\mathbf{kq},\Lambda}, u_{\mathbf{kq},\Lambda}, v_{\mathbf{kq},\Lambda}, \alpha_{\mathbf{k}_1\mathbf{k}\mathbf{k}_2,\lambda}, \beta_{\mathbf{k}_1\mathbf{k}\mathbf{k}_2,\lambda}\} = 0. \tag{B43}$$

By integrating the full set of renormalization equations between Λ and $\lambda = 0$, one is led to the fully renormalized one-particle operators

$$\tilde{e}^\dagger_{\mathbf{k}} = \tilde{x}_{\mathbf{k}} e^\dagger_{\mathbf{k}} + \frac{1}{\sqrt{N}}\sum_{\mathbf{q}} \tilde{t}_{\mathbf{k-q,q}} h_{-\mathbf{q}} : \psi^\dagger_{\mathbf{k-q}} : + \frac{1}{N}\sum_{\mathbf{k}_1\mathbf{k}_2} \tilde{\alpha}_{\mathbf{k}_1\mathbf{k}\mathbf{k}_2} : e^\dagger_{\mathbf{k}_1} h^\dagger_{\mathbf{k}_2} h_{\mathbf{k}_1+\mathbf{k}_2-\mathbf{k}} : , \tag{B44}$$

$$\tilde{h}^\dagger_{\mathbf{k}} = \tilde{y}_{\mathbf{k}} h^\dagger_{\mathbf{k}} + \frac{1}{\sqrt{N}}\sum_{\mathbf{q}} \tilde{u}_{\mathbf{q},-\mathbf{k}} e_{\mathbf{q-k}} : \psi^\dagger_{\mathbf{q}} : + \frac{1}{N}\sum_{\mathbf{k}_1\mathbf{k}_2} \tilde{\beta}_{\mathbf{k}_1\mathbf{k}_2,\mathbf{k}-\mathbf{k}_1+\mathbf{k}_2} : e^\dagger_{\mathbf{k}_1} e_{\mathbf{k}_2} h^\dagger_{\mathbf{k}-\mathbf{k}_1+\mathbf{k}_2} : , \tag{B45}$$

$$\tilde{\psi}^\dagger_{\mathbf{k}} = \tilde{z}_{\mathbf{k}} \psi^\dagger_{\mathbf{k}} + \frac{1}{\sqrt{N}}\sum_{\mathbf{q}} \tilde{v}_{\mathbf{kq}} : e^\dagger_{\mathbf{q+k}} h^\dagger_{-\mathbf{q}} : . \tag{B46}$$

Again, tilde symbols denote the fully renormalized quantities. With Eqs. (B44)–(B46) the expectation values $n^e_{\mathbf{k}}$, $n^h_{\mathbf{k}}$, $d_{\mathbf{k}}$, and $n^{\psi}_{\mathbf{k}}$ can be evaluated. Thus, for the fermionic quantities one obtains up to order $O(g^2_{\mathbf{k}})$ and $O(U^2_{\mathbf{k}})$

$$n^e_{\mathbf{k}} = |\tilde{x}_{\mathbf{k}}|^2 \tilde{n}^e_{\mathbf{k}} + \frac{1}{N}\sum_{\mathbf{q}} |\tilde{t}_{\mathbf{k-q,q}}|^2\big(1 - \tilde{n}^h_{-\mathbf{q}}\big)\tilde{n}^{\psi}_{\mathbf{k-q}} + \frac{1}{N^2}\sum_{\mathbf{k}_1\mathbf{k}_2}|\tilde{\alpha}_{\mathbf{k}_1\mathbf{k}\mathbf{k}_2}|^2 \tilde{n}^e_{\mathbf{k}_1}\tilde{n}^h_{\mathbf{k}_2}\big(1-\tilde{n}^h_{\mathbf{k}_1+\mathbf{k}_2-\mathbf{k}}\big), \tag{B47}$$

$$n^h_{\mathbf{k}} = |\tilde{y}_{\mathbf{k}}|^2 \tilde{n}^h_{\mathbf{k}} + \frac{1}{N}\sum_{\mathbf{q}} |\tilde{u}_{\mathbf{q},-\mathbf{k}}|^2\big(1 - \tilde{n}^e_{\mathbf{q-k}}\big)\tilde{n}^{\psi}_{\mathbf{q}} + \frac{1}{N^2}\sum_{\mathbf{k}_1\mathbf{k}_2}\big|\tilde{\beta}_{\mathbf{k}_1\mathbf{k}_2,\mathbf{k}-\mathbf{k}_1+\mathbf{k}_2}\big|^2 \tilde{n}^h_{\mathbf{k}_1-\mathbf{k}_1+\mathbf{k}_2}\tilde{n}^c_{\mathbf{k}_1}\big(1-\tilde{n}^c_{\mathbf{k}_2}\big), \tag{B48}$$

$$d_{\mathbf{k}} = x_{\mathbf{k}} y_{\mathbf{k}} \langle e^\dagger_{\mathbf{k}} h^\dagger_{-\mathbf{k}}\rangle_{\tilde{\mathcal{H}}} - \frac{1}{N^2}\sum_{\mathbf{k}_1\mathbf{k}_2} \tilde{\alpha}_{\mathbf{k}_1\mathbf{k},\mathbf{k}-\mathbf{k}_1+\mathbf{k}_2}\tilde{\beta}_{\mathbf{k}_1\mathbf{k}_2,\mathbf{k}-\mathbf{k}_1+\mathbf{k}_2}\tilde{n}^e_{\mathbf{k}_1} \times \big(1 - \tilde{n}^h_{\mathbf{k}-\mathbf{k}_1+\mathbf{k}_2}\big)\langle e^\dagger_{\mathbf{k}_2} h^\dagger_{-\mathbf{k}_2}\rangle_{\tilde{\mathcal{H}}}. \tag{B49}$$

On the right-hand sides the expectation values, formed with $\tilde{\mathcal{H}}$, can easily be evaluated:

$$\tilde{n}^e_{\mathbf{k}} = \xi^2_{\mathbf{k}} f\big(\tilde{E}^1_{\mathbf{k}}\big) + \eta^2_{\mathbf{k}} f\big(\tilde{E}^2_{\mathbf{k}}\big), \tag{B50}$$

$$\tilde{n}^h_{\mathbf{k}} = 1 - \eta^2_{\mathbf{k}} f\big(\tilde{E}^1_{\mathbf{k}}\big) - \xi^2_{\mathbf{k}} f\big(\tilde{E}^2_{\mathbf{k}}\big), \tag{B51}$$

$$\langle e^\dagger_{\mathbf{k}} h^\dagger_{-\mathbf{k}}\rangle_{\tilde{\mathcal{H}}} = \mathrm{sgn}\big(\tilde{E}^1_{\mathbf{k}} - \tilde{E}^2_{\mathbf{k}}\big)\big[f\big(\tilde{E}^1_{\mathbf{k}}\big) - f\big(\tilde{E}^2_{\mathbf{k}}\big)\big]\frac{\tilde{\Delta}_{\mathbf{k}}}{W_{\mathbf{k}}}, \tag{B52}$$

where $f(E)$ is the Fermi function. The prefactors $\xi_{\mathbf{k}}$ and $\eta_{\mathbf{k}}$ are the coefficients from the Bogoliubov transformation (B24).

Finally, the bosonic expectation value $n^{\psi}_{\mathbf{q}}$ is given by

$$n^{\psi}_{\mathbf{q}} = \langle \delta\psi^\dagger_{\mathbf{q}}\delta\psi_{\mathbf{q}}\rangle = \langle \psi^\dagger_{\mathbf{q}}\psi_{\mathbf{q}}\rangle - \langle\psi^\dagger_{\mathbf{q}}\rangle\langle\psi_{\mathbf{q}}\rangle\delta_{\mathbf{q=0}}, \tag{B53}$$

where from (B46)

$$\langle \psi^\dagger_{\mathbf{q}}\psi_{\mathbf{q}}\rangle = |\tilde{z}_{\mathbf{q}}|^2\langle \psi^\dagger_{\mathbf{q}}\psi_{\mathbf{q}}\rangle_{\tilde{\mathcal{H}}} + \frac{1}{N}\sum_{\mathbf{k}}|\tilde{v}_{\mathbf{qk}}|^2 \tilde{n}^h_{-\mathbf{k}}\tilde{n}^e_{\mathbf{k+q}}, \tag{B54}$$

$$\langle\psi^\dagger_{\mathbf{q}}\rangle \simeq \tilde{z}_{\mathbf{q}}\langle\psi^\dagger_{\mathbf{q}}\rangle_{\tilde{\mathcal{H}}}. \tag{B55}$$

Note that in $\langle\psi^\dagger_{\mathbf{q}}\rangle$ a smaller contribution from (B46) has been neglected. Thus,

$$n^{\psi}_{\mathbf{q}} = |\tilde{z}_{\mathbf{q}}|^2(\langle \psi^\dagger_{\mathbf{q}}\psi_{\mathbf{q}}\rangle_{\tilde{\mathcal{H}}} - \langle\psi^\dagger_{\mathbf{q}}\rangle_{\tilde{\mathcal{H}}}\langle\psi_{\mathbf{q}}\rangle_{\tilde{\mathcal{H}}}) + \frac{1}{N}\sum_{\mathbf{k}}|\tilde{v}_{\mathbf{qk}}|^2 \tilde{n}^h_{-\mathbf{k}}\tilde{n}^e_{\mathbf{k+q}}, \tag{B56}$$

where the expectation values on the right-hand side are formed with $\tilde{\mathcal{H}}$. With Eq. (B4) they become

$$\langle \psi^\dagger_{\mathbf{q}}\psi_{\mathbf{q}}\rangle_{\tilde{\mathcal{H}}} = \langle \Psi^\dagger_{\mathbf{q}}\Psi_{\mathbf{q}}\rangle_{\tilde{\mathcal{H}}} - \frac{\sqrt{N}\tilde{\Gamma}}{\tilde{\omega}_{\mathbf{q}}}\langle\Psi^\dagger_{\mathbf{q}} + \Psi_{\mathbf{q}}\rangle_{\tilde{\mathcal{H}}}\delta_{\mathbf{q},\mathbf{0}} + \frac{N\tilde{\Gamma}^2}{\tilde{\omega}^2_{\mathbf{k}}}\delta_{\mathbf{k},\mathbf{0}} = p(\tilde{\omega}_{\mathbf{q}}) + \frac{N\tilde{\Gamma}^2}{\tilde{\omega}^2_{\mathbf{q}}}\delta_{\mathbf{q},\mathbf{0}} \tag{B57}$$

and

$$\langle\psi^\dagger_{\mathbf{q}}\rangle_{\tilde{\mathcal{H}}} = \left[\langle\Psi^\dagger_{\mathbf{q}}\rangle_{\tilde{\mathcal{H}}} - \frac{\sqrt{N}\,\tilde{\Gamma}}{\tilde{\omega}_{\mathbf{q}}}\right]\delta_{\mathbf{q},\mathbf{0}} = -\frac{\sqrt{N}\,\tilde{\Gamma}}{\tilde{\omega}_{\mathbf{q}}}\delta_{\mathbf{q},\mathbf{0}}, \tag{B58}$$

where we have used $\langle\Psi^\dagger_{\mathbf{q}}\rangle_{\tilde{\mathcal{H}}} = 0$, and $p(\tilde{\omega}_{\mathbf{q}})$ is the bosonic distribution function. Inserting Eqs. (B57) and (B58) into (B56), one finally arrives at

$$n^{\psi}_{\mathbf{q}} = |\tilde{z}_{\mathbf{q}}|^2 p(\tilde{\omega}_{\mathbf{q}}) + \frac{1}{N}\sum_{\mathbf{k}}|\tilde{v}_{\mathbf{qk}}|^2 \tilde{n}^h_{-\mathbf{k}}\tilde{n}^e_{\mathbf{k+q}}, \tag{B59}$$

and similarly

$$\tilde{n}^{\psi}_{\mathbf{q}} = \langle \delta\psi^\dagger_{\mathbf{q}}\delta\psi_{\mathbf{q}}\rangle_{\tilde{\mathcal{H}}} \approx p(\tilde{\omega}_{\mathbf{q}}). \tag{B60}$$

Obviously, the electronic order parameter $d_{\mathbf{k}}$ and the photonic order parameter $\tilde{\Delta}_{\mathbf{k}}$ are intimately related. Due to (B49) and (B52), $d_{\mathbf{k}}$ is proportional to $\tilde{\Delta}_{\mathbf{k}}$, so that both order parameters are mutually dependent.

Note that in Sec. IV the numerical outcome of $n^e_{\mathbf{k}}$ and $n^h_{\mathbf{k}}$ will turn out to be the same. The reason for this is the assumed symmetric dispersions for the electron and hole bands in Eq. (2), $\varepsilon^e_{\mathbf{k}} = \varepsilon^h_{\mathbf{k}}$. As a consequence, also the original Hamiltonian (1) shows a certain symmetry: Replacing all electron operators $e^{(\dagger)}_{\mathbf{k}}$ by hole operators $h^{(\dagger)}_{\mathbf{k}}$ and vice versa, Hamiltonian (1) remains the same, except of the sign of the prefactor g, i.e.,

$$\mathcal{H}(\{e^{(\dagger)}_{\mathbf{k}}\},\{h^{(\dagger)}_{\mathbf{k}}\},g,U) = \mathcal{H}(\{h^{(\dagger)}_{\mathbf{k}}\},\{e^{(\dagger)}_{\mathbf{k}}\},-g,U). \quad \text{(B61)}$$

A closer inspection shows that the former ansatz (B31) for $e^{\dagger}_{\mathbf{k}}(\lambda)$ can be transformed to the ansatz (B32) for $h^{\dagger}_{\mathbf{k}}(\lambda)$. The same is true for the corresponding renormalization equations of the prefactors in Eqs. (B44) and (B45). Note that the property $n^e_{\mathbf{k}} = n^h_{\mathbf{k}}$ would no longer be valid in case different dispersions $\varepsilon^e_{\mathbf{k}} \neq \varepsilon^h_{\mathbf{k}}$ are used. However, also for the latter case the above renormalization equations remain valid.

APPENDIX C: LUMINESCENCE FUNCTIONS

Let us first evaluate the response function for the excitonic polarization (25) which reads as after the unitary invariance has been employed

$$A(\mathbf{k},\omega) = \frac{1}{2\pi}\int_{-\infty}^{\infty} \langle [\tilde{b}_{\mathbf{k}}(t),\tilde{b}^{\dagger}_{\mathbf{k}}]_-\rangle_{\tilde{\mathcal{H}}}\, e^{i\omega t}\, dt. \quad \text{(C1)}$$

The expectation value is formed with the fully renormalized Hamiltonian $\tilde{\mathcal{H}}$. The quantity $\tilde{b}^{\dagger}_{\mathbf{k}}$ is the transformed exciton creation operator

$$\tilde{b}^{\dagger}_{\mathbf{k}} = \frac{1}{\sqrt{N}}\sum_{\mathbf{p}} \tilde{e}^{\dagger}_{\mathbf{k}+\mathbf{p}}\tilde{h}^{\dagger}_{-\mathbf{p}}, \quad \text{(C2)}$$

where the unitary transformation has been applied separately to the two one-particle operators $\tilde{e}^{\dagger}_{\mathbf{k}}$ and $\tilde{h}^{\dagger}_{\mathbf{k}}$. Inserting Eqs. (B44) and (B45) into expressions (C1) and (C2), one obtains for $A(\mathbf{k},\omega)$

$$A(\mathbf{k},\omega) = A^{\mathrm{coh}}(\mathbf{k},\omega) + A^{\mathrm{inc}}(\mathbf{k},\omega), \quad \text{(C3)}$$

where the two parts will henceforth be denoted as coherent and incoherent. The coherent part is given by

$$\begin{aligned} A^{\mathrm{coh}}(\mathbf{k},\omega) = \frac{1}{N}\sum_{\mathbf{p}} |\tilde{x}_{\mathbf{k}+\mathbf{p}}\tilde{y}_{-\mathbf{p}}|^2 \big\{ &|\xi_{\mathbf{k}+\mathbf{p}}\eta_{\mathbf{p}}|^2 \big[f(\tilde{E}^1_{\mathbf{p}}) - f(\tilde{E}^1_{\mathbf{k}+\mathbf{p}})\big]\delta(\omega - \tilde{E}^1_{\mathbf{k}+\mathbf{p}} + \tilde{E}^1_{\mathbf{p}}) \\ &+ |\eta_{\mathbf{k}+\mathbf{p}}\eta_{\mathbf{p}}|^2\big[f(\tilde{E}^1_{\mathbf{p}}) - f(\tilde{E}^2_{\mathbf{k}+\mathbf{p}})\big]\delta(\omega - \tilde{E}^2_{\mathbf{k}+\mathbf{p}} + \tilde{E}^1_{\mathbf{p}}) + |\xi_{\mathbf{k}+\mathbf{p}}\xi_{\mathbf{p}}|^2\big[f(\tilde{E}^2_{\mathbf{p}}) - f(\tilde{E}^1_{\mathbf{k}+\mathbf{p}})\big]\delta(\omega - \tilde{E}^1_{\mathbf{k}+\mathbf{p}} + \tilde{E}^2_{\mathbf{p}}) \\ &+ |\eta_{\mathbf{k}+\mathbf{p}}\xi_{\mathbf{p}}|^2\big[f(\tilde{E}^2_{\mathbf{p}}) - f(\tilde{E}^2_{\mathbf{k}+\mathbf{p}})\big]\delta(\omega - \tilde{E}^2_{\mathbf{k}+\mathbf{p}} + \tilde{E}^2_{\mathbf{p}})\big\}. \end{aligned} \quad \text{(C4)}$$

It follows from the dominant contributions $\propto \tilde{x}_{\mathbf{k}} e^{\dagger}_{\mathbf{k}}$ and $\propto \tilde{y}_{\mathbf{k}} h^{\dagger}_{\mathbf{k}}$ in Eqs. (B44) and (B45). In addition, the one-particle operators $e^{(\dagger)}_{\mathbf{k}}$ and $h^{(\dagger)}_{\mathbf{k}}$ have to be expressed by the dynamical eigenvectors $C^{1,2}_{\mathbf{k}}$, which lead to the appearance of the Bogoliubov coefficients $\xi_{\mathbf{k}}$ and $\eta_{\mathbf{k}}$ in Eq. (C4).

The incoherent part $A^{\mathrm{inc}}(\mathbf{k},\omega)$ of the response function (C1) reads as to order $\mathcal{O}(g^2)$ and $\mathcal{O}(U^2)$

$$\begin{aligned} A^{\mathrm{inc}}(\mathbf{k},\omega) = \Pi^0_{\mathbf{k}}\delta[\omega - \tilde{\omega}(\mathbf{k})] - \frac{1}{N}\sum_{\mathbf{p}} \Pi^1_{\mathbf{pk}}\delta\big[\omega - E^1_{\mathbf{p}}(\mathbf{k})\big] + \frac{1}{N^2}\sum_{i,\mathbf{pk}_1} \Pi^{2,i}_{\mathbf{pk}_1,\mathbf{k}}\delta\big[\omega - E^{2,i}_{\mathbf{pk}_1}(\mathbf{k})\big] \\ + \frac{1}{N^3}\sum_{i,\mathbf{pk}_1\mathbf{k}_2} \Pi^{3,i}_{\mathbf{pk}_1\mathbf{k}_2,\mathbf{k}}\delta\big[\omega - E^{3,i}_{\mathbf{pk}_1\mathbf{k}_2}(\mathbf{k})\big], \end{aligned} \quad \text{(C5)}$$

with

$$E^1_{\mathbf{p}}(\mathbf{k}) = \tilde{\varepsilon}^e_{\mathbf{k}+\mathbf{p}} + \tilde{\varepsilon}^h_{-\mathbf{p}}, \quad \text{(C6)}$$

$$E^{2,1}_{\mathbf{pk}_1}(\mathbf{k}) = \tilde{\varepsilon}^h_{-\mathbf{p}} - \tilde{\varepsilon}^h_{-\mathbf{k}_1} + \tilde{\omega}_{\mathbf{k}+\mathbf{p}-\mathbf{k}_1}, \quad \text{(C7)}$$

$$E^{2,2}_{\mathbf{pk}_1}(\mathbf{k}) = \tilde{\varepsilon}^e_{\mathbf{k}+\mathbf{p}} - \tilde{\varepsilon}^e_{\mathbf{p}+\mathbf{k}_1} + \tilde{\omega}_{\mathbf{p}}, \quad \text{(C8)}$$

$$E^{3,1}_{\mathbf{pk}_1\mathbf{k}_2}(\mathbf{k}) = \tilde{\varepsilon}^h_{-\mathbf{p}} - \tilde{\varepsilon}^h_{\mathbf{k}_1-\mathbf{k}_2-\mathbf{k}-\mathbf{p}} + \tilde{\varepsilon}^h_{\mathbf{k}_2} + \tilde{\varepsilon}^e_{\mathbf{k}_1}, \quad \text{(C9)}$$

$$E^{3,2}_{\mathbf{pk}_1\mathbf{k}_2}(\mathbf{k}) = \tilde{\varepsilon}^h_{-\mathbf{p}-\mathbf{k}_1+\mathbf{k}_2} - \tilde{\varepsilon}^e_{\mathbf{k}_2} + \tilde{\varepsilon}^e_{\mathbf{k}_1} + \tilde{\varepsilon}^e_{\mathbf{k}+\mathbf{p}}, \quad \text{(C10)}$$

and

$$\Pi^0_{\mathbf{k}} = \frac{2}{N^2}\sum_{\mathbf{pk}_1}\tilde{x}_{\mathbf{k+p}}\tilde{y}_{-\mathbf{k}_1}\tilde{u}_{\mathbf{kp}}\tilde{t}_{\mathbf{kk}_1}\tilde{n}^e_{\mathbf{p+k}}\big(1-\tilde{n}^h_{-\mathbf{k}_1}\big), \tag{C11}$$

$$\begin{aligned}\Pi^1_{\mathbf{p}}(\mathbf{k}) = {}& 2\tilde{x}_{\mathbf{k+p}}\tilde{y}_{-\mathbf{k}}\frac{1}{N}\sum_{\mathbf{k}_1}\big[\tilde{x}_{\mathbf{k}_1+\mathbf{k}}\tilde{\beta}_{\mathbf{k+p},\mathbf{k}_1+\mathbf{k},-\mathbf{p}}\tilde{n}^e_{\mathbf{k}_1+\mathbf{k}} - \tilde{y}_{-\mathbf{k}_1}\alpha_{\mathbf{k+p},\mathbf{k}_1+\mathbf{k},-\mathbf{p}}\big(1-\tilde{n}^h_{-\mathbf{k}_1}\big)\big]\big(1-\tilde{n}^e_{\mathbf{k}_1}-\tilde{n}^h_{-\mathbf{p}}\big)\\
&+\frac{1}{N^2}\sum_{\mathbf{k}_1\mathbf{k}_2}\big\{2\tilde{x}_{\mathbf{k+p}}\tilde{y}_{-\mathbf{p}}\alpha_{\mathbf{k}_2,\mathbf{k}_1+\mathbf{k},-\mathbf{p}}\beta_{\mathbf{k+p},\mathbf{k}_2,-\mathbf{k}-\mathbf{p}+\mathbf{k}_2-\mathbf{k}_1}\tilde{n}^e_{\mathbf{k}_2}\big(1-\tilde{n}^h_{-\mathbf{k}-\mathbf{p}+\mathbf{k}_2-\mathbf{k}_1}\big)\\
&+2\tilde{x}_{\mathbf{k}_1+\mathbf{k}}\tilde{y}_{-\mathbf{k}_1}\tilde{\alpha}_{\mathbf{k+p},\mathbf{k}_1+\mathbf{k},-\mathbf{p}}\tilde{\beta}_{\mathbf{k+p},\mathbf{k}_2+\mathbf{k},-\mathbf{p}}\big(1-\tilde{n}^h_{-\mathbf{p}}\big)\tilde{n}^e_{\mathbf{k}_2+\mathbf{k}}\\
&-\tilde{y}_{-\mathbf{k}_1}\tilde{y}_{-\mathbf{k}_2}\tilde{\alpha}_{\mathbf{k+p},\mathbf{k}_1+\mathbf{p},-\mathbf{p}}\tilde{\alpha}_{\mathbf{k+p},\mathbf{k}_2+\mathbf{k},-\mathbf{p}}b\big(1-\tilde{n}^h_{-\mathbf{p}}\big)\big(1-\tilde{n}^h_{-\mathbf{k}_2}\big)\\
&-\tilde{x}_{\mathbf{k+p}}\tilde{x}_{\mathbf{k}_2+\mathbf{k}}\tilde{\beta}_{\mathbf{k}_1,\mathbf{k+p},-\mathbf{k}_1+\mathbf{k}}\tilde{\beta}_{\mathbf{k}_1,\mathbf{k}_2+\mathbf{k},-\mathbf{k}_2+\mathbf{k}}n^e_{\mathbf{k}_2+\mathbf{k}}\tilde{n}^e_{\mathbf{k+p}}\big\}\big(1-\tilde{n}^e_{\mathbf{k+p}}-\tilde{n}^h_{-\mathbf{p}}\big),\end{aligned} \tag{C12}$$

$$\Pi^{2,1}_{\mathbf{pk}_1,\mathbf{k}} = \big|\tilde{y}_{-\mathbf{p}}\tilde{t}_{\mathbf{k+p}-\mathbf{k}_1,\mathbf{k}_1}\big|^2\big[\tilde{n}^h_{-\mathbf{k}_1}\big(1-\tilde{n}^h_{-\mathbf{p}}\big)-\tilde{n}^\psi_{\mathbf{k+p}-\mathbf{k}_1}\big(\tilde{n}^h_{-\mathbf{k}_1}-\tilde{n}^h_{-\mathbf{p}}\big)\big], \tag{C13}$$

$$\Pi^{2,2}_{\mathbf{pk}_1,\mathbf{k}} = \big|\tilde{x}_{\mathbf{k+p}}\tilde{u}_{\mathbf{k}_1\mathbf{p}}\big|^2\big[\tilde{n}^e_{\mathbf{k+p}}\big(1-\tilde{n}^e_{\mathbf{p}+\mathbf{k}_1}\big)-\tilde{n}^\psi_{\mathbf{k}_1}\big(\tilde{n}^e_{\mathbf{p}+\mathbf{k}_1}-\tilde{n}^e_{\mathbf{k+p}}\big)\big], \tag{C14}$$

$$\begin{aligned}\Pi^{3,1}_{\mathbf{pk}_1\mathbf{k}_2,\mathbf{k}} = {}&\big(\big|\tilde{y}_{-\mathbf{p}}\tilde{\alpha}_{\mathbf{k}_1,\mathbf{k+p},\mathbf{k}_2}\big|^2-\tilde{y}_{-\mathbf{p}}\tilde{y}_{\mathbf{k}_2}\alpha_{\mathbf{k}_1,\mathbf{k+p},\mathbf{k}_2}\tilde{\alpha}_{\mathbf{k}_1,-\mathbf{k}_2+\mathbf{k},-\mathbf{p}}\big)\\
&\times\big[\big(1-\tilde{n}^e_{\mathbf{k}_1}\big)\big(1-\tilde{n}^h_{-\mathbf{p}}\big)\big(\tilde{n}^h_{\mathbf{k}_1+\mathbf{k}_2-\mathbf{k}-\mathbf{p}}-\tilde{n}^h_{-\mathbf{k}_1}\big)+\tilde{n}^h_{\mathbf{k}_2}\big(1-\tilde{n}^h_{\mathbf{k}_1+\mathbf{k}_2-\mathbf{k}-\mathbf{p}}\big)\big(1-\tilde{n}^e_{\mathbf{k}_1}-\tilde{n}^h_{-\mathbf{p}}\big)\big],\end{aligned} \tag{C15}$$

$$\begin{aligned}\Pi^{3,2}_{\mathbf{pk}_1\mathbf{k}_2,\mathbf{k}} = {}&\big(\big|\tilde{x}_{\mathbf{k+p}}\tilde{\beta}_{\mathbf{k}_1\mathbf{k}_2,-\mathbf{p}-\mathbf{k}_1+\mathbf{k}_2}\big|^2-\tilde{x}_{\mathbf{k+p}}\tilde{x}_{\mathbf{k}_1}\beta_{\mathbf{k}_1\mathbf{k}_2,-\mathbf{p}-\mathbf{k}_1+\mathbf{k}_2}\tilde{\beta}_{\mathbf{k+p},\mathbf{k}_2,-\mathbf{p}-\mathbf{k}_1+\mathbf{k}_2}\big)\\
&\times\big[\tilde{n}^e_{\mathbf{k+p}}\tilde{n}^h_{-\mathbf{p}-\mathbf{k}_1+\mathbf{k}_2}\big(\tilde{n}^e_{\mathbf{k+p}}-\tilde{n}^e_{\mathbf{k}_2}\big)+\tilde{n}^e_{\mathbf{k}_2}\big(1-\tilde{n}^e_{\mathbf{k}_1}\big)\big(1-\tilde{n}^e_{\mathbf{k+p}}-\tilde{n}^h_{-\mathbf{p}-\mathbf{k}_1+\mathbf{k}_2}\big)\big].\end{aligned} \tag{C16}$$

Again, all expectation values on the right-hand sides are formed with the renormalized Hamiltonian $\tilde{\mathcal{H}}$. Note that for simplicity $A^{\mathrm{inc}}(\mathbf{p},\omega)$ was calculated without use of the Bogoliubov transformation (B24). The reason for this approximation results from the fact that $A^{\mathrm{inc}}(\mathbf{p},\omega)$ turns out to be quite small compared to the coherent part of $A(\mathbf{k},\omega)$. Moreover, the additional sums in Eq. (C11) tend to cover the influence of $\tilde{\Delta}_{\mathbf{k}}$ in $W_{\mathbf{k}}$ [compare Eq. (B28)].

Finally, we consider the response function for the cavity photon mode

$$B(\mathbf{q},\omega) = \frac{1}{2\pi}\int_{-\infty}^{\infty}\langle[\tilde{\psi}_{\mathbf{q}}(t),\tilde{\psi}^\dagger_{\mathbf{q}}]_-\rangle_{\tilde{\mathcal{H}}}\,e^{i\omega t}dt, \tag{C17}$$

where $\tilde{\psi}^\dagger_{\mathbf{q}}$ is again the fully renormalized quantity. According to (B46) we have

$$\tilde{\psi}^\dagger_{\mathbf{q}} = \tilde{z}_{\mathbf{q}}\psi^\dagger_{\mathbf{q}} + \tfrac{1}{\sqrt{N}}\textstyle\sum_{\mathbf{k}}\tilde{v}_{\mathbf{qk}} : e^\dagger_{\mathbf{q+k}}h^\dagger_{-\mathbf{k}} : . \tag{C18}$$

Using Eqs. (24) and (B29), one easily finds

$$\begin{aligned}B(\mathbf{q},\omega) = {}&|\tilde{z}_{\mathbf{q}}|^2\delta(\omega-\tilde{\omega}_{\mathbf{q}}) + \frac{1}{N}\sum_{\mathbf{k}}|\tilde{v}_{\mathbf{qk}}|^2\big\{|\xi_{\mathbf{k+q}}\eta_{\mathbf{k}}|^2\big[f\big(\tilde{E}^1_{\mathbf{k}}\big)-f\big(\tilde{E}^1_{\mathbf{k+q}}\big)\big]\delta\big(\omega-\tilde{E}^1_{\mathbf{k+q}}+\tilde{E}^1_{\mathbf{k}}\big)\\
&+|\eta_{\mathbf{k+q}}\eta_{\mathbf{k}}|^2\big[f\big(\tilde{E}^1_{\mathbf{k}}\big)-f\big(\tilde{E}^2_{\mathbf{k+q}}\big)\big]\delta\big(\omega-\tilde{E}^2_{\mathbf{k+q}}+\tilde{E}^1_{\mathbf{k}}\big)+|\xi_{\mathbf{k+q}}\xi_{\mathbf{k}}|^2\big[f\big(\tilde{E}^2_{\mathbf{k}}\big)-f\big(\tilde{E}^1_{\mathbf{k+q}}\big)\big]\delta\big(\omega-\tilde{E}^1_{\mathbf{k+q}}+\tilde{E}^2_{\mathbf{k}}\big)\\
&+|\eta_{\mathbf{k+q}}\xi_{\mathbf{k}}|^2\big[f\big(\tilde{E}^2_{\mathbf{k}}\big)-f\big(\tilde{E}^2_{\mathbf{k+q}}\big)\big]\delta\big(\omega-\tilde{E}^2_{\mathbf{k+q}}+\tilde{E}^2_{\mathbf{k}}\big)\big\}.\end{aligned} \tag{C19}$$

Note that, apart from the first δ function and the prefactor under the sum, the result for $B(\mathbf{q},\omega)$ resembles that of the coherent contribution $A^{\mathrm{coh}}(\mathbf{k},\omega)$ of the excitonic polarization.

[1] *Bose-Einstein Condensation*, edited by A. Griffin, D. W. Snoke, and S. Stringari (Cambridge University Press, Cambridge, 1995).

[2] S. A. Moskalenko and D. W. Snoke, *Bose-Einstein Condensation of Excitons and Biexcitons* (Cambridge University Press, Cambridge, 2000).

[3] J. M. Blatt, K. W. Böer, and W. Brandt, Phys. Rev. **126**, 1691 (1962).

[4] S. A. Moskalenko, Fiz. Tverd. Tela **4**, 276 (1962) [Sov. Phys. Solid State **4**, 199 (1962)].

[5] P. B. Littlewood, P. R. Eastham, J. M. J. Keeling, F. M. Marchetti, B. D. Simons, and M. H. Szymanska, J. Phys.: Condens. Matter **16**, S3597 (2004).

[6] H. Stolz, R. Schwartz, F. Kieseling, S. Som, M. Kaupsch, S. Sobkowiak, D. Semkat, N. Naka, T. Koch *et al.*, New J. Phys. **14**, 105007 (2012).

[7] N. F. Mott, Philos. Mag. **6**, 287 (1961).

[8] R. Knox, in *Solid State Physics*, edited by F. Seitz and D. Turnbull (Academic, New York, 1963), Suppl. 5, p. 100.

[9] B. I. Halperin and T. M. Rice, in *Solid State Physics*, edited by F. Seitz, D. Turnbull, and H. Ehrenreich (Academic, New York, 1967), Vol. 21, p. 115.
[10] F. X. Bronold and H. Fehske, Phys. Rev. B **74**, 165107 (2006).
[11] B. Zenker, D. Ihle, F. X. Bronold, and H. Fehske, Phys. Rev. B **85**, 121102R (2012).
[12] B. Bucher, P. Steiner, and P. Wachter, Phys. Rev. Lett. **67**, 2717 (1991).
[13] Y. Wakisaka, T. Sudayama, K. Takubo, T. Mizokawa, M. Arita, H. Namatame, M. Taniguchi, N. Katayama, M. Nohara, and H. Takagi, Phys. Rev. Lett. **103**, 026402 (2009).
[14] C. Monney, E. F. Schwier, M. G. Garnier, N. Mariotti, C. Didiot, H. Cercellier, J. Marcus, H. Berger, A. N. Titov, H. Beck *et al.*, New J. Phys. **12**, 125019 (2010).
[15] H. Deng, G. Weihs, C. Santori, J. Bloch, and Y. Yamamoto, Science **298**, 199 (2002).
[16] J. Kasprzak, M. Richard, S. Kundermann, A. Baas, P. Jeambrun, J. M. J. Keeling, F. M. Marchetti, M. H. Szymańska, R. André, J. L. Staehli, V. Savona *et al.*, Nature (London) **443**, 409 (2006).
[17] H. Deng, H. Haug, and Y. Yamamoto, Rev. Mod. Phys. **82**, 1489 (2010).
[18] K. Kamide and T. Ogawa, Phys. Rev. B **83**, 165319 (2011).
[19] T. Byrnes, N. Y. Kim, and Y. Yamamoto, Nat. Phys. **10**, 803 (2014).
[20] H. Shi, G. Verechaka, and A. Griffin, Phys. Rev. B **50**, 1119 (1994).
[21] B. Laikhtman, Europhys. Lett. **43**, 53 (1998).
[22] H. Stolz and D. Semkat, Phys. Rev. B **81**, 081302 (2010).
[23] P. R. Eastham and P. B. Littlewood, Phys. Rev. B **64**, 235101 (2001).
[24] A. S. Aleksandrov, V. F. Elesin, A. N. Kremlin, and V. P. Yakovlev, Zh. Eksp. Teor. Fiz. **72**, 1913 (1977) [Sov. Phys. JETP **45**, 1005 (1977)].
[25] K. W. Becker, A. Hübsch, and T. Sommer, Phys. Rev. B **66**, 235115 (2002).
[26] V. N. Phan, K. W. Becker, and H. Fehske, Phys. Rev. B **81**, 205117 (2010).
[27] N. V. Phan, H. Fehske, and K. W. Becker, Europhys. Lett. **95**, 17006 (2011).
[28] M. H. Szymańska, J. Keeling, and P. B. Littlewood, Phys. Rev. Lett. **96**, 230602 (2006).
[29] J. Keeling, P. R. Eastham, M. H. Szymanska, and P. B. Littlewood, Phys. Rev. B **72**, 115320 (2005).
[30] A. Chiocchetta and I. Carusotto, Phys. Rev. A **90**, 023633 (2014).
[31] S. Sykora, A. Hübsch, K. W. Becker, G. Wellein, and H. Fehske, Phys. Rev. B **71**, 045112 (2005).
[32] S. Sykora, K. W. Becker, and H. Fehske, Phys. Rev. B **81**, 195127 (2010).